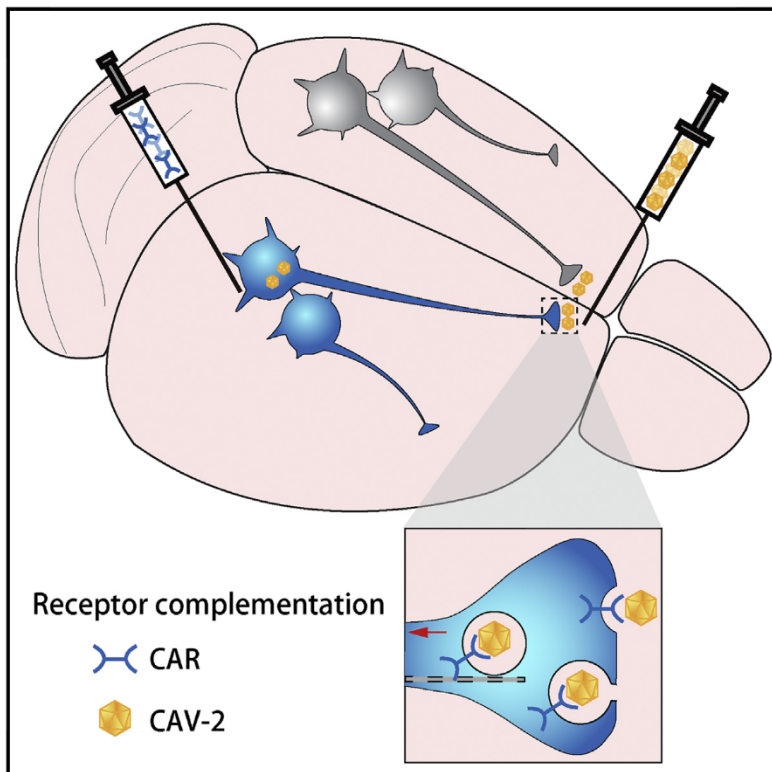


A Viral Receptor Complementation Strategy to Overcome CAV-2 Tropism for Efficient Retrograde Targeting of Neurons

Graphical Abstract



Authors

Shu-Jing Li, Alexander Vaughan,
James Fitzhugh Sturgill, Adam Kepcs

Correspondence

kepecs@cshl.edu

In Brief

Retrograde viruses are indispensable tools for linking neural connectivity with function; however, their use is often limited by poor or variable infectivity. Li et al. report a viral receptor complementation strategy for more efficient and tropism-free projection-specific neuronal targeting.

Highlights

- A receptor complementation strategy enables tropism-free retrograde viral delivery
- Enhanced CAV-2 retrograde spread in long-range projections in both mice and rats
- Vectors delivering CAR and different cargos for anatomical and functional studies



A Viral Receptor Complementation Strategy to Overcome CAV-2 Tropism for Efficient Retrograde Targeting of Neurons

Shu-Jing Li,¹ Alexander Vaughan,¹ James Fitzhugh Sturgill,¹ and Adam Kepecs^{1,2,*}

¹Cold Spring Harbor Laboratory, Cold Spring Harbor, NY 11724, USA

²Lead Contact

*Correspondence: kepecs@cshl.edu

<https://doi.org/10.1016/j.neuron.2018.05.028>

SUMMARY

Retrogradely transported neurotropic viruses enable genetic access to neurons based on their long-range projections and have become indispensable tools for linking neural connectivity with function. A major limitation of viral techniques is that they rely on cell-type-specific molecules for uptake and transport. Consequently, viruses fail to infect variable subsets of neurons depending on the complement of surface receptors expressed (viral tropism). We report a receptor complementation strategy to overcome this by potentiating neurons for the infection of the virus of interest—in this case, canine adenovirus type-2 (CAV-2). We designed AAV vectors for expressing the coxsackievirus and adenovirus receptor (CAR) throughout candidate projection neurons. CAR expression greatly increased retrograde-labeling rates, which we demonstrate for several long-range projections, including some resistant to other retrograde-labeling techniques. Our results demonstrate a receptor complementation strategy to abrogate endogenous viral tropism and thereby facilitate efficient retrograde targeting for functional analysis of neural circuits.

INTRODUCTION

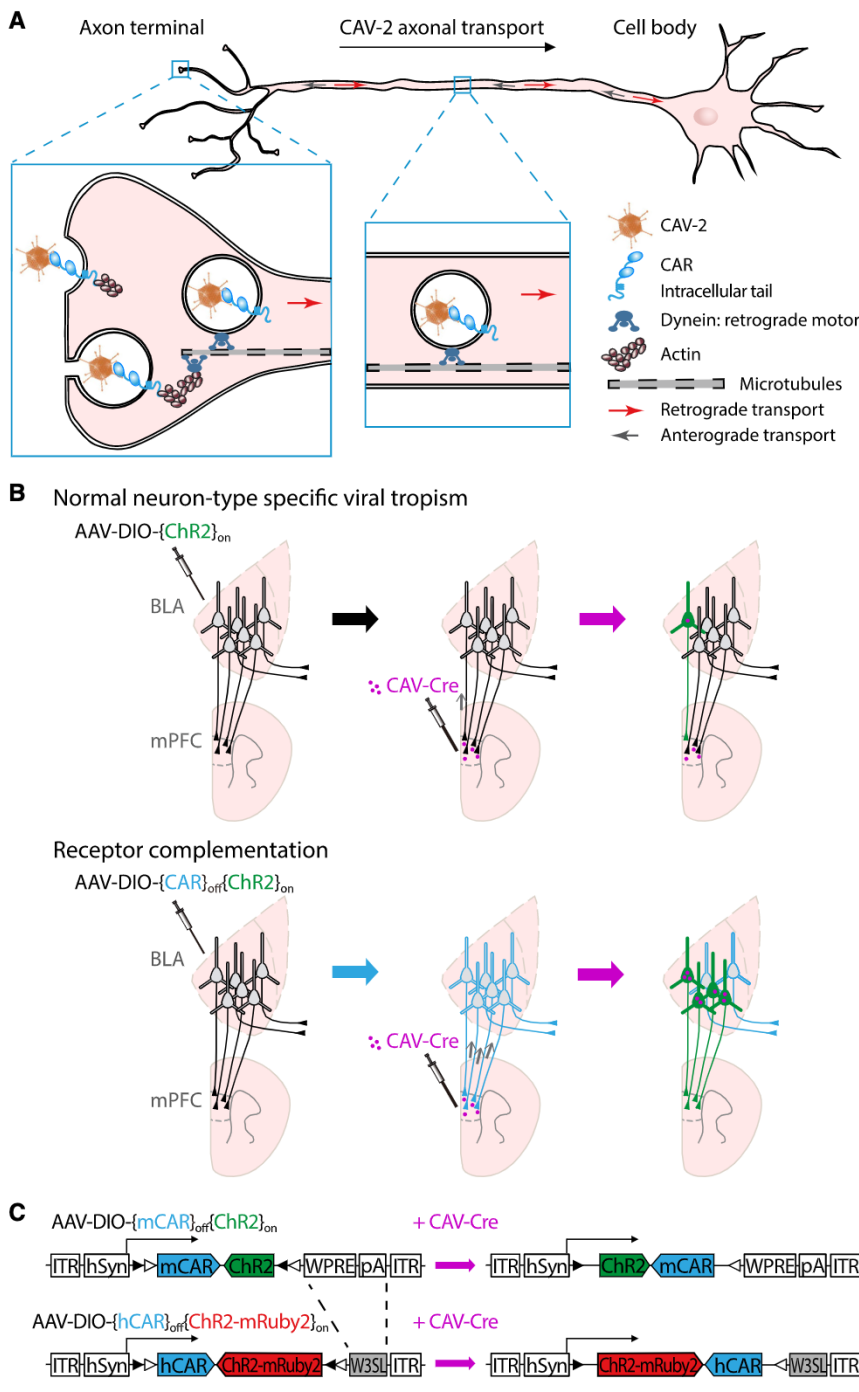
Deciphering how neural circuits are anatomically organized is fundamental to understanding how the brain processes information. However, linking identified neural types with known connectivity to their functional properties has been a major challenge largely due to the paucity of techniques available for selectively targeting specific neuronal subtypes. While classic neuroanatomical tracers have yielded information about the architectural principles of connectivity between different brain regions, they cannot deliver genetic materials that would enable their use beyond anatomical mapping (Katz et al., 1984; Luppi et al., 1990; Schmued and Fallon, 1986; Wan et al., 1982).

Neurotropic viruses have emerged as powerful tools to overcome the limitations of classic tracers. Recombinant viral vectors

can carry the flexible and relatively large transgene cargos used for neurophysiological experiments, including effectors or indicators of neural activity, DNA recombinases, and fluorescent proteins (Nassi et al., 2015; Ugolini, 2010). A particularly valuable approach is labeling neurons based on their long-range axonal projections via retrograde viruses, such as rabies virus (Callaway and Luo, 2015; Ugolini, 1995; Wall et al., 2010; Wickersham et al., 2007), retrograde adeno-associated virus (rAAV2-retro) (Tervo et al., 2016), herpes simplex virus 1 (HSV) (Frampton et al., 2005; Ugolini et al., 1987; Lilley et al., 2001), the herpes virus known as pseudorabies virus (PRV) (Aston-Jones and Card, 2000; Boldogkoi et al., 2009; Oyibo et al., 2014), and canine adenovirus type 2 (CAV-2) (Boender et al., 2014; Carter et al., 2013; Junyent and Kremer, 2015; Soudais et al., 2001). Retrograde viruses hijack normal cellular machinery to enter axon terminals and travel back to the soma. Virus injected in one area can travel through axons to label cell bodies from many brain regions. An unfortunate drawback of viral techniques is that they require neurons to express specific molecules for viral uptake and transport. Since the expression of the requisite receptors varies by cell type and can be developmentally regulated, viral infection and transport can be biased to specific neuronal types (Grove and Marsh, 2011; Mateo et al., 2015; Schneider-Schaulies, 2000). With this variable viral uptake, or “tropism,” it is difficult to achieve reliable labeling, recording, or manipulation in every cell type or to interpret negative results in anatomical studies. Indeed, absence of evidence is not evidence of absence: due to viral tropism, unobserved pathways may simply be unlabeled. Until now, this has been a serious caveat for viral tracing techniques that seek to reveal anatomical ground truth.

To address this challenge, we developed a receptor complementation strategy to mitigate the tropism of a commonly used retrograde virus, CAV-2. CAV-2 has many advantages, including relatively low immunogenicity (Perreau and Kremer, 2005), long-term duration of transgene expression in mammalian brain (Soudais et al., 2004), preferential transduction of neurons (Soudais et al., 2001; Zussy et al., 2016), efficient retrograde transport from axon terminal to soma (Salinas et al., 2009; Soudais et al., 2001), and large cloning capacity (Soudais et al., 2004). CAV-2 has been used in numerous studies to label long-range projections (Ekstrand et al., 2014; Junyent and Kremer, 2015). CAV-2 is commonly used as part of a dual viral system in which CAV-2 expressing Cre recombinase is injected into putative target areas and an AAV expressing Cre-dependent cargo (e.g.,





channelrhodopsin 2 [ChR2]) is injected into candidate source regions. In this configuration CAV-2 retrogradely travels from distal axon terminals to the soma and expresses Cre recombinase in the nucleus, turning on the expression of ChR2 only in those neurons projecting from source to target. This dual viral system has been used in many studies to selectively target a defined pathway in behaving animals (Beyeler et al., 2016; Carter et al., 2013; Darvas and Palmiter, 2009; Hnasko et al., 2006; Kim et al., 2015; Ruder et al., 2016; Senn et al., 2014; Wu et al., 2012).

Figure 1. CAR Complementation Strategy and Vector Design

(A) CAR mediates CAV-2 binding, internalization, and retrograde transport (after Henaff and Salinas, 2010).

(B) Schematic description of the relationship between receptor expression and retrograde gene transfer efficiency under normal neuron-type specific viral tropism or receptor complementation.

(C) AAV constructs carry mCAR or hCAR and inverted cargo genes (ChR2-HA or ChR2-mRuby2) that are switched by the presence of Cre. ITR, inverted terminal repeat; hSyn, human synapsin 1 promoter; WPRE, woodchuck hepatitis B virus post-transcriptional element; pA, polyadenylation elements; W3SL, a shortened version of WPRE and polyadenylation elements. Open and filled triangles, incompatible lox sites (loxP and lox272).

Although CAV-2 is a powerful tool for studying neural circuits, its use is also limited by tropism. For instance, Senn and colleagues showed that in the basolateral amygdala (BLA) to medial prefrontal cortex (mPFC) pathway, CAV-2 only infected a subpopulation of mPFC-projecting BLA neurons, while another retrograde virus (HSV) infected a more lateral population of BLA neurons (Senn et al., 2014).

To overcome CAV-2 tropism, we took advantage of well-understood molecular mechanisms for its internalization and axonal transport. Coxsackievirus and adenovirus receptor (CAR) is a conserved cell surface adhesion molecule and functions as the receptor for CAV-2 (Bergelson et al., 1997, 1998; Soudais et al., 2000, 2001). The extracellular domain of CAR mediates the binding and docking of CAV-2 to the neuronal membrane, while the intracellular tail of CAR is required for the internalization, endocytosis, and axonal transport of CAV-2 (Salinas et al., 2009, 2014) (Figure 1A). Notably, in the adult brain, CAR is predominantly enriched at the presynaptic boutons (Zussy et al., 2016).

We designed AAV constructs to express CAR and thereby potentiate CAV-2 infection in candidate projection neurons. To show the utility of this approach, we demonstrated the enhancement of the CAV-2 retrograde labeling rate in multiple long-range-projecting neural circuits in both mice and rats, providing a robust method for high-efficiency, tropism-free retrograde labeling. In addition, we generated a toolkit of CAR-expressing vectors to carry different cargos useful for anatomical and functional studies of neural circuit. We used the CAR/CAV-2 dual viral

Table 1. List of AAV Vectors Containing CAR and Other Cargos

Name	Cre-OFF	Cre-ON	Backbone	Addgene Cat #
AAV-DIO-{ChR2}on	–	ChETA-HA	hSyn-DIO-WPRE	111386
AAV-DIO-{mCAR}off{ChR2}on	mCAR-Myc	ChETA-HA	hSyn-DIO-WPRE	111387
AAV-DIO-{hCAR}off{ChR2}on	hCAR-Myc	ChETA-HA	hSyn-DIO-WPRE	111388
AAV-DIO-{ChR2-mRuby2}on-W3SL	–	ChETA-mRuby2	hSyn-DIO-W3SL	111389
AAV-DIO-{mCAR}off{ChR2-mRuby2}on-W3SL	mCAR-Myc	ChETA-mRuby2	hSyn-DIO-W3SL	111390
AAV-DIO-{hCAR}off{ChR2-mRuby2}on-W3SL	hCAR-Myc	ChETA-mRuby2	hSyn-DIO-W3SL	111391
AAV-DIO-{hCAR}off{ChR2-EYFP}on-W3SL	hCAR-Myc	ChETA-EYFP	hSyn-DIO-W3SL	111392
AAV-DIO-{mCAR}off{GCaMP6f}on	mCAR-Myc	GCamp6f	hSyn-DIO-WPRE	111393
AAV-DIO-{hCAR}off{GCaMP6f}on-W3SL	hCAR-Myc	GCamp6f	hSyn-DIO-W3SL	111394
AAV-DIO-{mCAR}off{DTR-GFP}on	mCAR-Myc	DTR-GFP	hSyn-DIO-WPRE	111395
AAV-DIO-{hCAR}off{DTR-GFP}on-W3SL	hCAR-Myc	DTR-GFP	hSyn-DIO-W3SL	111396
AAV-DIO-{hCAR}off{hM4Di-mCherry}on-W3SL	hCAR-Myc	hM4Di-mCherry	hSyn-DIO-W3SL	111397

system to deliver GCaMP6f in specific pathways and showed calcium responses in behaving mice in CAR-potentiated neurons, demonstrating the compatibility of the CAR/CAV-2 dual viral system with other cargos for *in vivo* functional studies.

RESULTS

CAR Complementation Strategy

We hypothesized that if the infection rate of CAV-2 is limited by neuronal CAR expression that enables internalization and axonal transport, we could then attenuate this tropism by overexpressing CAR in candidate projection neurons. The potentiation of projection neurons with CAR is expected to facilitate the attachment and internalization of CAV-2 as well as the retrograde axonal transport of CAV-2 (Figures 1A and 1B).

We developed a CAR complementation strategy as part of a Cre-dependent dual viral system to enable the conditional expression of various cargos in the CAR-expressing vector by a special Cre-Switch design (Figure 1C). In one configuration, coding sequences for CAR and ChR2 are positioned back to back in forward and inverted orientations, respectively, flanked by double-floxed inverse open reading frames (DIOs) in a recombinant AAV vector (Atasoy et al., 2008; Gunaydin et al., 2010; Schnütgen et al., 2003). In this configuration, Myc-labeled mouse CAR (mCAR) is expressed by default in a Cre-OFF manner, while the hemagglutinin (HA)-tagged ChR2 variant ChETA is packaged in a Cre-ON manner (Bergelson et al., 1998; Gunaydin et al., 2010). After infection with this AAV-DIO-{mCAR}off{ChR2}on virus at the source region, candidate projection neurons express mCAR throughout soma and fibers and are thereby potentiated for CAV-2 infection. Following CAV-Cre injection at the putative target region, CAR expression promotes the uptake of CAV-2 into the fiber terminals and the retrograde axonal transport of CAV-2 back to the distally located soma and results in Cre recombinase expression at the source region. In turn, the Cre recombinase inverts the DIO cassette, halting expression of mCAR and instead inducing expression of the ChR2 cargo (Figures 1B and 1C). This approach has two important advantages: first, it allows for more robust and reliable expression of the inverted transgenes compared to strategies

for expressing both proteins in series (e.g., IRES or 2A), and second, it circumvents concerns that sustained CAR expression might interfere with neuronal function.

We generated a toolkit of vectors containing CAR and different cargos that are useful for anatomical and functional studies of neural circuits, including fluorescent proteins (e.g., mRuby2 and EYFP), effectors of neural activity (e.g., light-gated ion channel ChETA and ligand-gated ion channel hM4Di), indicators of neural activity (e.g., calcium indicator GCamp6f), and methods for cell ablation (e.g., diphtheria toxin receptor [DTR]) (Chen et al., 2013; Gunaydin et al., 2010; Saito et al., 2001) (Table 1). Because the AAV genome has a limited packaging capacity of ~4.7 kb, there are strong constraints on the architecture of this vector. In order to integrate multiple cargos simultaneously into the same vector, we chose a short human synapsin I (hSyn; ~0.5 kb) promoter, which confers neuron-specific long-term transgene expression (Kügler et al., 2003). This backbone is referred to as hSyn-DIO-WPRE. We replaced the WPRE and hGH polyadenylation elements with a shorter regulatory cassette (W3SL) built from a shortened WPRE, an upstream element, and SV40 late polyadenylation signal (Choi et al., 2014). This W3SL cassette allows 0.7 kb additional cloning capacity and shows comparable expression efficiency with conventional WPRE and polyadenylation cassettes. This backbone is referred to as hSyn-DIO-W3SL. Besides the mouse CAR, we also tested the human homolog hCAR (Bergelson et al., 1997), which has about 83% sequence identity to mCAR, to serve as a foreign variant that may have less potential for endogenous function (Figure 1C; Table 1).

Receptor Complementation Strategy Improves Retrograde Spread of CAV-2 in Mice

To assess whether CAR complementation promotes the infection and labeling efficiency of CAV-2, we first tested our AAV vectors in the BLA-to-mPFC pathway (BLA → mPFC), where CAV-2 is known to have limited infectivity (Senn et al., 2014). We injected the AAV-DIO-{mCAR}off{ChR2}on virus in BLA in one hemisphere and a control vector AAV-DIO-{ChR2}on without CAR in the contralateral BLA. After 6–8 days of mCAR expression, a mixture of CAV-dsRed, CAV-Cre, and a conventional retrograde tracer cholera toxin subunit B (CTB) (Luppi et al.,

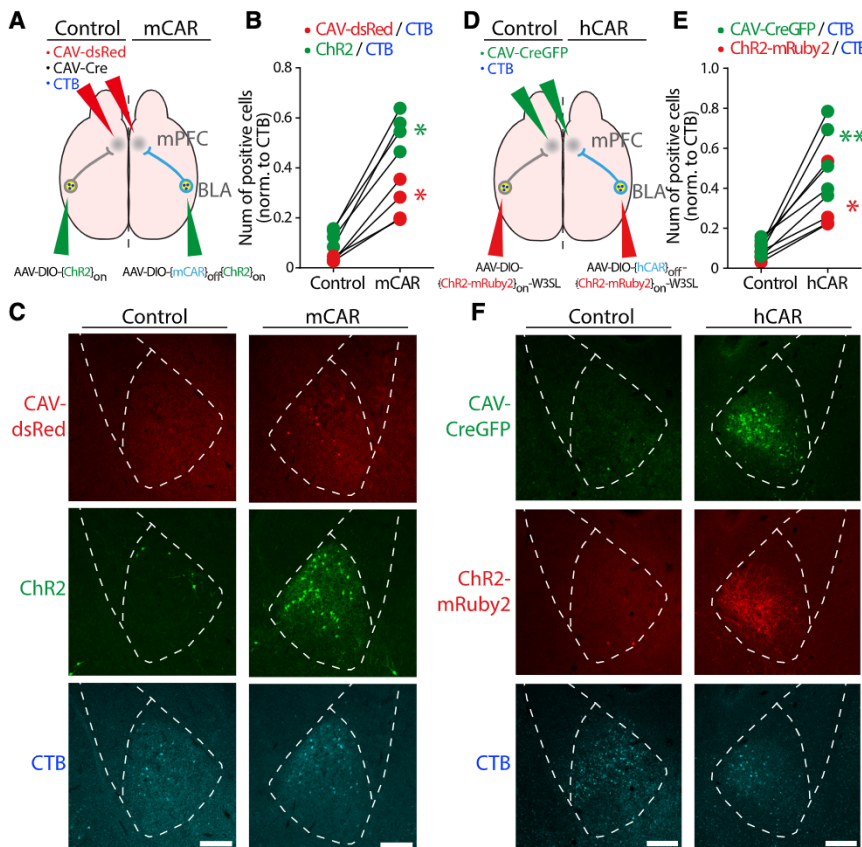


Figure 2. CAR Enhances Infection Rates of CAV-2 in BLA-to-mPFC Projections in Mice

(A) Schematic of an experiment testing the efficiency of receptor complementation using mCAR in the BLA → mPFC pathway.

(B) Plot of infection rates reflecting the number of positive cells of CAV-dsRed/CTB and ChR2/CTB in BLA under control and mCAR+ conditions. Contralateral hemispheres in each animal are paired by lines. n = 4 mice, Mann-Whitney U test, *p < 0.05 for both CAV-dsRed and ChR2.

(C) Representative immunofluorescent images of CAV-dsRed (red), ChR2 (green, labeled by HA tag), and CTB (cyan) in BLA under control and mCAR+ conditions. Scale bars, 200 μm.

(D) Schematic of an experiment testing the efficiency of receptor complementation using alternate vector carrying hCAR along with a larger cargo capacity.

(E) As in (B) except plotting of CAV-CreGFP/CTB and ChR2-mRuby2/CTB in BLA under control and hCAR+ conditions. n = 5 mice, **p < 0.01 for CAV-CreGFP; n = 4 mice, *p < 0.05 for ChR2-mRuby2.

(F) As in (C) except showing CAV-CreGFP (green), ChR2-mRuby2 (red), and CTB (cyan) in BLA under control and hCAR+ conditions.

1990; Wan et al., 1982) was injected bilaterally in mPFC (Figure 2A; Figure S1). After an additional 8–10 days post infection, we quantified the number of dsRed-, ChR2-, and CTB-positive cells in BLA for both CAR+ and control hemispheres within each brain slice. In this experiment, the number of dsRed-expressing cells in BLA reflects the overall infection rate and retrograde labeling efficiency of CAV-dsRed, whereas the number of ChR2-expressing neurons in BLA reflects the level of Cre-dependent recombination arising from CAV-Cre. Both measures were normalized to the number of cells labeled with CTB to minimize the potential bias and variance induced by injection location or volume. As a control, we observed that the location and spread of CAV-2/CTB injections from each animal showed no apparent bias between CAR+ and control hemispheres (Figure S1).

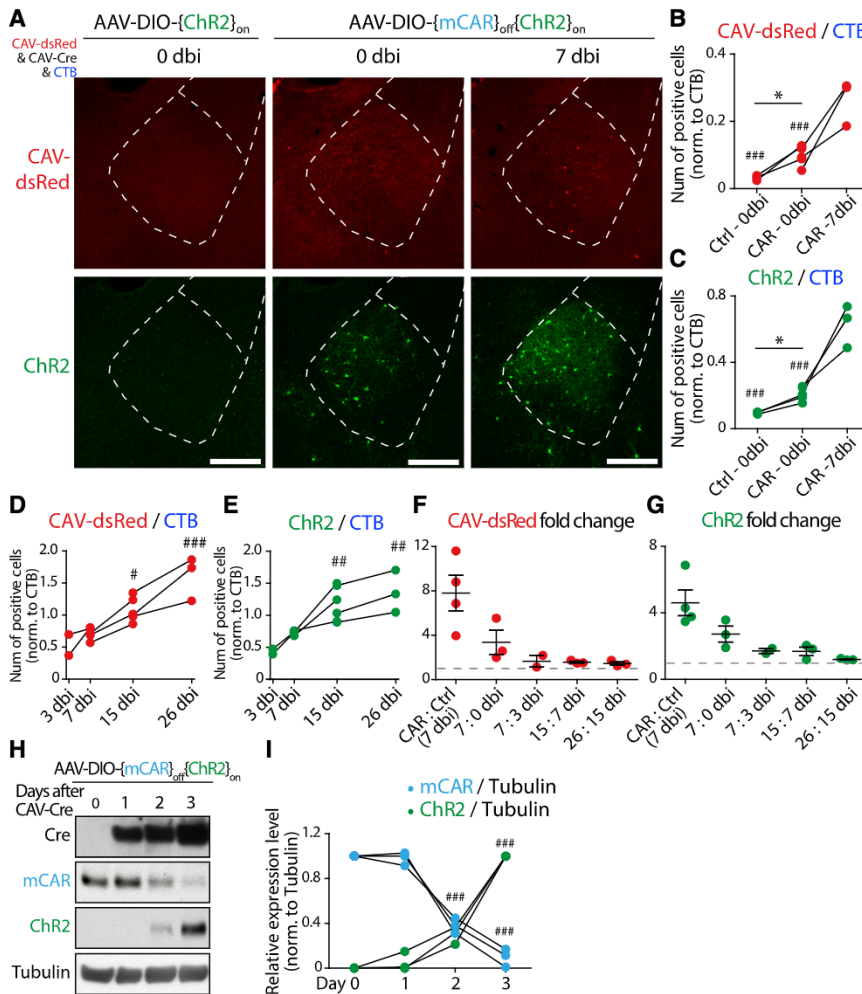
As we expected, in the control hemisphere, expression of both CAV-dsRed and CAV-Cre-induced ChR2 were very low in BLA neurons, which reflects the tropism of CAV-2 in this pathway (Senn et al., 2014). In contrast, in the CAR+ hemisphere, expression of both CAV-dsRed (4- to 12-fold higher) and CAV-Cre (3- to 7-fold higher) were significantly increased. The control retrograde tracer CTB was approximately equal in labeling efficiency across hemispheres (Figures 2B, 2C, 3F, and 3G).

To confirm that the increase in ChR2 expression following CAR complementation arose from Cre-dependent expression rather than leakiness, we investigated the expression patterns of CAR, Cre, and ChR2 in BLA with or without the injection of

CAV-Cre in mPFC. In animals without CAV-Cre injection, there was significant expression of mCAR but no leaky expression of ChR2, validating the Cre dependency of our expression system.

In animals injected with CAV-Cre, ChR2-positive cells were frequently co-localized with CRE protein, and in those cells, the expression of mCAR dropped or completely shut down, consistent with our Cre-Switch design (Figures S2A and S2B).

We also showed that an alternate vector carrying human CAR along with a larger cargo capacity (i.e., AAV-DIO-(hCAR)_{off}{ChR2-mRuby2}_{on}-W3SL) enables higher CAV-2 infection. For these experiments, a mixture of CAV-CreGFP and CTB was injected bilaterally into mPFC, with infectivity quantified as the number of GFP- or mRuby2-positive cells normalized by the number of CTB-positive cells (Figure 2D; Figure S1). As shown in Figures 2E and 2F, the hCAR+ hemisphere exhibited a higher rate of CAV-CreGFP infectivity (3- to 9-fold greater) and Cre-dependent mRuby2 expression (3- to 7-fold greater) compared to the contralateral hemisphere injected with empty control vector AAV-DIO-(ChR2-mRuby2)_{on}. The similar results using mouse and human CAR variants suggest that the function of CAR as a CAV-2 receptor is conserved across mammalian species. As expected, no leaky expression of mRuby2 was observed in CAV-CreGFP-negative animals. In animals injected with CAV-CreGFP, mRuby2 fluorescence was co-localized with CAV-CreGFP, and in those neurons, hCAR expression was turned off (Figures S2C and S2D). Together, these results demonstrate that the CAR complementation strategy significantly promotes the efficacy of CAV-2 as a retrograde viral vector in mice.

**Figure 3. Time Course of CAR Expression**

(A) Representative images showing the expression of CAV-dsRed (red) and ChR2 (green) in BLA with or without a delay period between control AAV, mCAR-expressing AAV, and CAV-2 injections (control with no delay: Ctrl-0dbi; CAR with no delay: CAR-0dbi; and CAR with 7-day delay: CAR-7dbi). Scale bars, 200 μ m.

(B) Plot of infection rates from the number of positive cells of CAV-dsRed/CTB in BLA under conditions described in (A). Contralateral hemispheres in each animal are paired by lines. One-way ANOVA, $p = 0.0001$; Tukey's multiple comparison test, *** $p < 0.001$ for both Ctrl-0dbi versus CAR-7dbi and CAR-0dbi versus CAR-7dbi. * $p < 0.05$ between Ctrl-0dbi and CAR-0dbi using paired t test, $n = 3$ mice.

(C) As in (B) except plotting of ChR2/CTB. One-way ANOVA, $p < 0.0001$; Tukey's multiple comparison test, *** $p < 0.001$ for both Ctrl-0dbi versus CAR-7dbi and CAR-0dbi versus CAR-7dbi. * $p < 0.05$ between Ctrl-0dbi and CAR-0dbi using paired t test, $n = 3$ mice.

(D) Plot of infection rates from the number of positive cells of CAV-dsRed/CTB in BLA under different dbi conditions. DsRed signals were greatly enhanced by anti-RFP antibody immunostaining; therefore, the relative ratio of CAV-dsRed versus CTB is higher than in (B). Contralateral hemispheres in each animal were paired by lines. n values represent the number of mice, one-way ANOVA, $p = 0.0002$; Tukey's multiple comparison test, * $p < 0.05$ for 3 dbi versus 15 dbi, *** $p < 0.001$ for 3 dbi versus 26 dbi.

(E) As in (D) except plotting of ChR2/CTB. One-way ANOVA, $p = 0.0011$; Tukey's multiple comparison test, ** $p < 0.01$ for both 3 dbi versus 15 dbi and 3 dbi versus 26 dbi.

(F and G) Fold changes of CAV-dsRed/CTB (F; $p = 0.0069$) and ChR2/CTB (G; $p = 0.0052$) between opposing hemispheres with 7-day delay

for CAR versus control and CAR injection at 7-day delay versus no delay or other different dbi conditions. The fold changes were decreasing and approaching to value 1 (dash line). Error bars, SEM; n values represent the number of mice; one-way ANOVA.

(H and I) Representative immunoblots (H) and quantitation (I) showing the expression patterns of Cre, mCAR, ChR2, and housekeeping gene Tubulin after CAV-Cre infection. mCAR levels at different post-infection days were normalized to day 0. $p < 0.0001$ using one-way ANOVA; Tukey's multiple comparison test, *** $p < 0.001$ for day 0 versus day 2 or day 3. ChR2 levels were normalized to day 3. $p < 0.0001$ using one-way ANOVA; Tukey's multiple comparison test, *** $p < 0.001$ for day 0 versus day 2 or day 3. $n = 3$ independent experiments.

Time Course of the Onset and Offset of CAR Protein Expression

The method proposed here requires an intrinsic time delay, as the synthesis and transport of CAR to distal axons is necessary to potentiate CAV-2 infection. To characterize this, we manipulated the relative timing of AAV-CAR and CAV-2 injections to identify the onset speed of CAR expression and the optimal delay between injections (dbi).

As a baseline, we first sought to establish the efficacy of simultaneous injection of AAV-CAR and CAV-2 (0 dbi). We injected control and CAR-expressing AAVs into BLA in opposing hemispheres, along with bilateral mPFC injection of CAV-dsRed, CAV-Cre and CTB on the same day (0 dbi). To our surprise, the CAR+ hemisphere still showed enhanced CAV-dsRed and CAV-Cre infections (Figures 3A–3C). Considering that the expression of CAR is terminated once a neuron is infected by

CAV-Cre, these results suggest that even an extremely short-term and low-level expression of CAR still benefits retrograde infectivity of CAV-2.

As expected, when this zero delay condition (0 dbi) was compared with 7 days' delay condition (7 dbi), the hemisphere with 7 dbi showed much higher infection rates for both CAV-dsRed and CAV-Cre (Figures 3A–3C). Thus, although brief expression of CAR is effective in supporting CAV-2 infection, a delay period allows higher CAR expression and transport to further improve CAV-2 retrograde labeling.

We determined the optimal delay period between AAV-CAR and CAV-2 injections by evaluating CAV-2 infection rates under different delay conditions (3 dbi, 7 dbi, 15 dbi, and 26 dbi). With more prolonged delays, the infectivity of CAV-2 rose further (3 dbi versus 7 dbi, 7 dbi versus 15 dbi) until it began to saturate after 2 weeks (15 dbi versus 26 dbi) (Figures 3D and 3E). To

reduce inter-animal variability in gene expression and histological processing, we paired the data from two opposing hemispheres of the same animal with staggered delay conditions and calculated the relative fold changes of CAV-2 infectivity. Quantifying the relative fold changes revealed a similar relationship: the enhancement in expression continued with increasing delay and saturated after 2 weeks (Figures 3F and 3G). Thus, a delay period of 2 weeks is likely sufficient to achieve nearly maximal level of CAR and potentiation of CAV-2 infection.

We next tested how fast Cre turned off CAR expression. To precisely and homogeneously control the timing of Cre expression in neurons, we performed this experiment in cultured primary neurons. First, CAR was introduced by transfecting neurons with AAV-DIO-{mCAR}_{off}{ChR2}_{on} construct, and then those neurons were infected by CAV-Cre and collected at different post-infection days for analysis of CAR expression. Immunoblot results showed that mCAR expression dropped within 2 days since its synthesis was halted by Cre, indicating that CAR protein half-life is similar to the median half-life of the endogenous proteome in human and mouse cells (Cambridge et al., 2011). In addition, similar to the results in Figure S2, the level of accumulated Cre-ON ChR2 protein was negatively correlated with that of mCAR, excluding the possibility of cell-death-induced protein reduction (Figures 3H and 3I).

CAR Complementation Promotes CAV-2 Infection and Retrograde Transgene Delivery in Rats

Given the challenges associated with generating transgenic rats, viral methods for transgene delivery in rats are particularly important. Therefore, we tested whether CAR complementation could overcome viral tropisms and enable robust retrograde labeling in rat projection neurons. We targeted the projection from the ventral hippocampus CA1 (vCA1) region to the mPFC (Figure S3A), which is known to be challenging for retrograde labeling (Dr. Thomas Klausberger, personal communication). Indeed, no retrograde signal was observed in vCA1 following injection of tracer CTB or wheat germ agglutinin (WGA) in mPFC (data not shown), and only a few vCA1 neurons were sparsely labeled with high concentration retrobeads (Figure S3B). Similarly, after injecting the control vector AAV-DIO-{ChR2}_{on} with no CAR in vCA1 and CAV-CreGFP in mPFC, GFP-positive or ChR2-positive CA1 pyramidal neurons were extremely sparse, indicating low CAV-2 infectivity. In contrast, potentiation with CAR significantly increased the number of GFP-positive and ChR2-positive CA1 pyramidal neurons (3- to 27-fold) (Figures S3B and S3C). However, CAR-potentiated labeling of the rat vCA1-mPFC pathway with CAV-CreGFP was not very dense, possibly because the human synapsin I promoter did not drive strong enough expression in rat CA1 pyramidal neurons. Indeed, we found that AAV-DIO-{mCAR}_{off}{ChR2}_{on} only expressed mCAR in a few CA1 pyramidal neurons (Figure S3D). In summary, these results show that CAR complementation works in rats as well as mice and can be used to gain genetic access to recalcitrant pathways such as the vCA1-mPFC projection.

CAR-Expressing AAV Boosts Overall CAV-Driven Expression Level in AAV Mixtures

One convenient feature of AAV vectors is their high multiplicity of infection, allowing co-infection of the same neuron by a mixture

of different AAVs (Miyamichi et al., 2013). With this in mind, we tested whether our AAV-CAR vector could be used as a “helper virus” alongside other AAVs to enhance overall CAV-driven expression levels.

To test this, we targeted neurons projecting from rat orbito-frontal cortex (OFC) to ventral striatum (VS). We injected a mixture of AAV-DIO-{mCAR}_{off}{ChR2}_{on} alongside an AAV carrying Cre-dependent Synaptophysin-mCherry (AAV-DIO-{SYN-mCherry}_{on}) (Garfield et al., 2014) into rat OFC and injected CAV-CreGFP in VS (Figure 4A). As shown in Figure 4B, we observed a higher infection rate for CAV-CreGFP in OFC in the CAR+ hemisphere. Importantly, the number of Synaptophysin-mCherry-positive cells and the signal intensity were also greatly enhanced on the same side, as compared to the contralateral hemisphere injected with a mixture of the control vector AAV-DIO-{ChR2}_{on} and AAV-DIO-{SYN-mCherry}_{on}. These results suggest that AAV-CAR can be used alongside other AAVs to enhance CAV-2 infection rates and overall retrograde activation of Cre-dependent AAVs.

The fusion of synaptophysin, a synaptic marker, with mCherry, a fluorescence protein, also enabled us to examine the morphology of the cell body, axons, and synapses of the labeled neurons. CAR-potentiated OFC neurons showed normal morphology, strong projections with dense arborization in VS of CAR+ hemisphere (Figure 4C). The density of synaptic puncta on axon fibers (number of puncta per unit length) in VS had no obvious changes in the CAR+ hemisphere compared to the control hemisphere, indicating a similar strength of synaptic connection and growth of neurites (Figure 4D). Other features of labeled neurons, including layer localization and gross morphology, appeared identical (Figure 4B). These results indicate that overexpression of CAR did not affect the morphology and wiring of neurons.

Efficiency of CAR/CAV-2 System in Dopaminergic Pathways

To show that CAR/CAV-2 provides access to cell populations difficult to target with alternative tools, we directly compared its performance with another retrograde viral reagent, rAAV2-retro. The newly developed retrograde AAV variant rAAV2-retro has the advantage of being a single-component system and also enables flexible and non-toxic retrograde transgene expression (Tervo et al., 2016). The retrograde infectivity of rAAV2-retro is due to its engineered capsid, which may not permit the infection of all neuron types. For example, rAAV2-retro has weak labeling efficiency in dopaminergic neurons projecting from the ventral tegmental area and substantia nigra pars compacta (VTA/SNC) to dorsal lateral striatum (DLS) (Tervo et al., 2016).

To determine whether CAR/CAV-2 can overcome these limitations, we directly compared the retrograde transport efficiency of CAR/CAV-2 with rAAV2-retro in VTA/SNC to DLS pathway (VTA/SNC → DLS). In VTA/SNC, we injected AAV-DIO-{mCAR}_{off}{ChR2}_{on} to potentiate neurons for CAV-2 infection and injected AAV-DIO-{SYN-mCherry}_{on} to monitor the efficiency of retrograde transport. In DLS, we injected Cre-expressing retrograde AAV (rAAV2-retro-Cre) and CAV-2 (CAV-Cre) at opposing hemispheres with CTB as a control (Figure 5A). We found that although rAAV2-retro-Cre infected numerous neurons at the injection site in DLS (shown by Cre-positive nuclei in DLS, Figure S4A), it

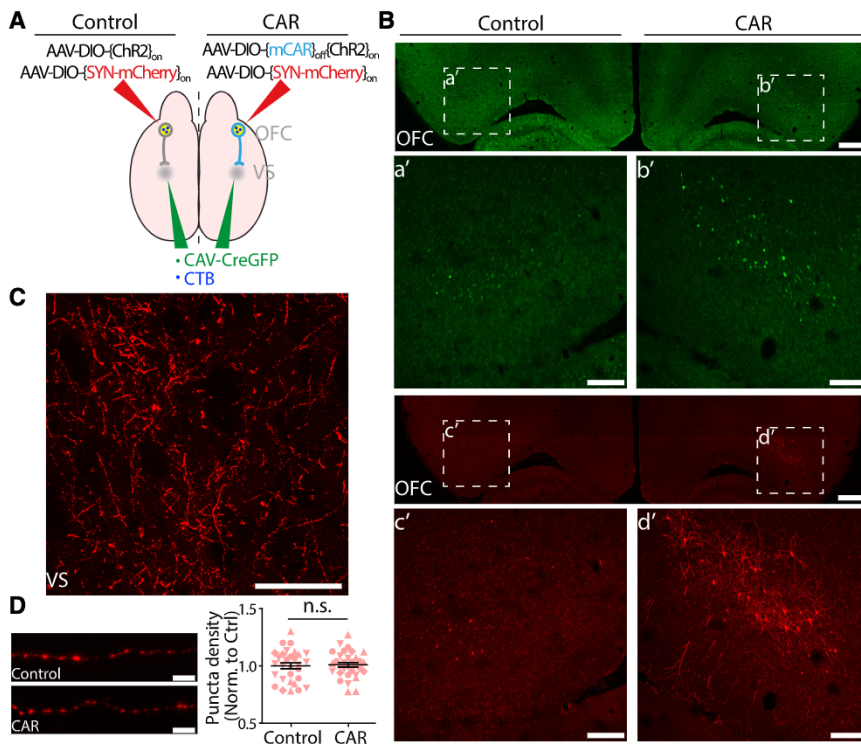


Figure 4. CAR-Expressing AAV Helps Enhance CAV-2-Driven Transgene Expression in AAV Mixtures

(A) Schematic of AAV and CAV-2 injections in OFC-to-VS pathway in rat.

(B) Representative immunofluorescent images of CAV-CreGFP (green) and Synaptophysin-mCherry (red) expression in OFC in control and CAR+ hemispheres. Scale bars of large view, 1 mm. Scale bars of enlarged view of OFC regions in a'-d', 200 μ m.

(C) Extensive labeling of axon fibers by Synaptophysin-mCherry in VS in the CAR+ hemisphere. Scale bars, 200 μ m.

(D) Left: representative enlarged images of synaptic puncta on the axon terminal fibers in VS in control and CAR+ hemispheres. Scale bars, 5 μ m. Right: quantification of puncta density (number of puncta per unit length) normalized to that of control hemisphere. Data are from four animals (each is presented by individual shape). Error bars, SEM; n values represent the number of fibers counted. Mann-Whitney U test, p = 0.8713. n.s., no significant difference.

showed only marginal retrograde transport to VTA/SNC and induced weak Synaptophysin-mCherry expression in VTA/SNC, consistent with previous reports (Tervo et al., 2016). In contrast, although CAV-Cre infected very few neurons at the injection site in DLS (which is advantageous because it reduces off-target expression), it robustly induced strong Synaptophysin-mCherry expression in TH-positive dopaminergic neurons in VTA/SNC, indicating its specific targeting of CAR+ neuron axons and efficient retrograde transport (Figures 5B–5D). These results demonstrate that the CAR/CAV-2 system provides access to label neuronal populations unaddressed by rAAV2-retro.

To alleviate concerns about potential CAV-2 immunogenicity and toxicity, we directly compared the toxicity of CAV-2 with rAAV2-retro by assaying cell apoptosis at the viral injection sites in DLS via TUNEL staining (terminal deoxynucleotidyl transferase dUTP nick end labeling). TUNEL-positive cells were rare at both CAV-2 and rAAV2-retro injection sites. No statistically significant difference of apoptosis was observed between CAV-2 and rAAV2-retro injection sites, although immune responses caused by surgical injuries may be difficult to distinguish from those potentially caused by viruses (Figure S4B). These results reveal that CAV-2 has low toxicity or immunogenicity in the brain, which is consistent with reports that CAV-2-infected neurons are able to survive for months or even more than a year in the rat brain (Burgos-Robles et al., 2017; Soudais et al., 2004).

Monitoring Neural Activity in Live Animals Using a CAR/CAV-2 System

Lastly, we used the CAR potentiation strategy to measure the functional properties of a previously difficult-to-target projection

pathway. We performed fiber photometry in mPFC-projecting BLA neurons, a method for collecting bulk intracellular calcium fluorescent signals through a single implanted multimode optical fiber. We designed a Cre-dependent calcium sensor construct, AAV-DIO-{hCAR}_{off}{GCaMP6f}_{on}-W3SL, and injected it into BLA in one hemisphere and a control vector, AAV-Flex-{GCaMP6f}_{on}-WPRE, into the contralateral BLA. After 7–8 days, CAV-Cre was injected in mPFC on both hemispheres to initiate GCaMP6f expression and turn off CAR expression in mPFC-projecting BLA neurons. Optical fibers were implanted in BLA to monitor neural activity through fiber photometry (Figures 6A and 6B). 6–7 weeks after completion of behavioral training and fiber photometry, we histologically confirmed correct fiber placements in BLA in both CAR+-potentiated and control hemispheres (Figure 6C). The control hemisphere showed only a few sparsely labeled neurons, which greatly limited the size of fluorescent signals and the neuronal responses to task events we observed. However, in the hemisphere where neurons were potentiated by CAR, a larger population of neurons was labeled by GCaMP6f and fluorescent signals were greatly enhanced (Figures 6C and 6D). Evaluation of GCaMP6f expression level in the entire BLA region in another animal without fiber implantation also confirmed a lower level of GCaMP6f labeling in control hemisphere (Figures S5A and S5B).

Motivated by the large body of work demonstrating the importance of the BLA in appetitive and aversive conditioning, we tested the response properties of mPFC-projecting BLA neurons in a series of head-fixed, classical conditioning tasks (Janak and Tye, 2015; Maren and Quirk, 2004; Rogan et al., 1997; Senn et al., 2014; Shabel and Janak, 2009). 3 weeks after CAV-Cre injections, mice were initially trained in a task wherein the presentation of one odor predicted water reward. We found that

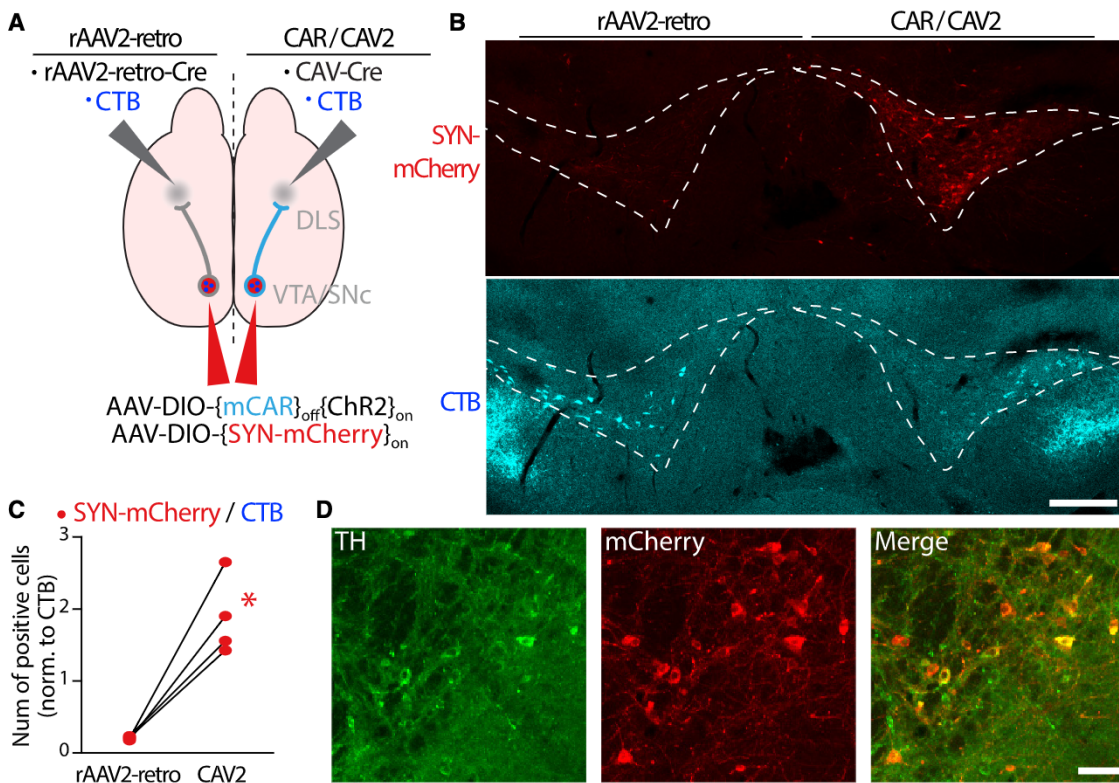


Figure 5. CAR/CAV-2 Dual Viral System Produces Robust Labeling in Striatal Dopaminergic Pathway

(A) Schematic of AAV, CAV-2, and rAAV2-retro injections in VTA/SNC to DLS projection.

(B) Representative immunofluorescent images of Synaptophysin-mCherry (red) and CTB (cyan) in VTA/SNC. Scale bars, 1 mm.

(C) Plot of infection rates from the number of positive cells of Synaptophysin-mCherry/CTB in VTA/SNC under conditions as in (A). Contralateral hemispheres in each animal are paired by lines. *p < 0.05 using Mann-Whitney U test, n = 4 mice.

(D) Representative immunofluorescent images of TH (green), Synaptophysin-mCherry (red), and overlay (Merge) in VTA/SNC showing that most of the Synaptophysin-mCherry-labeled neurons are TH-positive dopamine neurons. Scale bars, 20 μ m.

CAR-potentiated BLA neurons responded strongly to the odor cue in the first few trials, but with repeated odor presentations the cue responses diminished (Figures 6E–6G). As the mouse began to lick in receipt of water reward, these neurons developed precisely timed responses to reward delivery. In contrast to their diminishing odor responses, their responses to water reward were consistently high across all the sessions (Figure 6H). After a few training days, the same animal was trained in a second task in which a second odor cue predicted an aversive air puff with a probability of 0.5. As before, responses of mPFC-projecting BLA neurons to odor cue 2 were evident across the first few trials but declined with prolonged exposure (Figures 6E and 6F). Moreover, these neurons also responded robustly to air puff punishment across all the sessions (Figure 6I). While, on average, mPFC-projecting BLA neurons responded only weakly to odor stimuli, examination of the first ten trials of each session revealed pronounced responses to the novel odorants (Figure 6F). Taken together, these results are consistent with the reported functional characteristics of BLA neurons: novelty responses to unfamiliar stimuli, habituation after repeated odor exposure, and activation toward reward and punishment (Burgos-Robles et al., 2017; Schoenbaum et al., 1999; Takahashi et al., 2005). Data from

another animal corroborated these findings: in the CAR+ hemisphere, the mPFC-projecting BLA population displayed strong initial responses to odorants as well as to reinforcements (water and air puff) (Figures S5C–S5I). In summary, these results show that CAR-potentiated neurons have robust functional responses to various behavioral events, with BLA \rightarrow mPFC neurons responding to novel sensory stimuli early. This demonstrates that the CAR/CAV-2 system enables *in vivo* functional characterization of anatomically defined populations in behaving animals.

DISCUSSION

Retrograde viruses have become essential reagents in the neuroscience toolkit, enabling the functional analysis of anatomically defined neural circuits. These viruses hijack intrinsic cellular mechanisms to enter neurons and travel through the axon to the cell body. The specific molecules required for viral uptake and transport can show variable expression across different neuronal types, leading to preferential labeling of some neuronal pathways over others. Such tropism can be advantageous if it happens to enable targeting of particular projections of interests, but in general, it limits the usefulness of viral

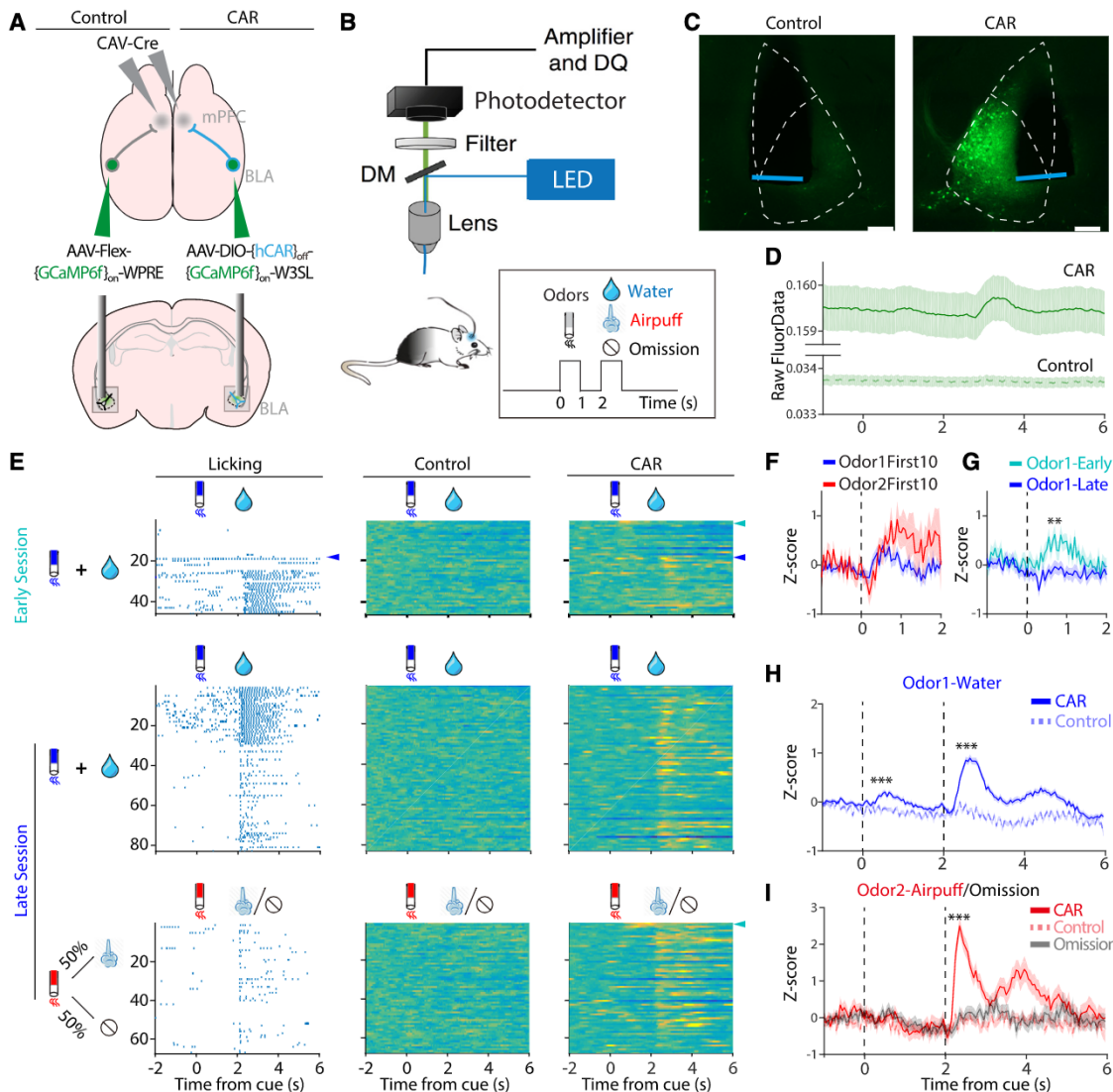


Figure 6. CAR-Expressing AAV Is an Effective Vector for Functional In Vivo Ca^{2+} Imaging

- (A) Schematic of AAV and CAV-2 viral injections and fiber implantations to visualize the neural activities of mPFC-projecting BLA neurons with GCaMP6f.
- (B) Schematic of *in vivo* fiber photometry of head-fixed mice under Pavlovian behavior tasks.
- (C) Verification of GCaMP6f expression levels and fiber positions in the animal from (D)–(I) after recordings. Blue lines indicate reconstructed positions of implanted fiber tips based on the insertion tracts. Scale bars, 200 μ m.
- (D) The raw fluorescent signals detected in control and CAR hemispheres before photo-bleaching correction and baseline normalization.
- (E) Rasters of licking (left) and GCaMP6f responses in mPFC-projecting BLA neurons in control (middle) and CAR+ (right) hemispheres of mice under Pavlovian tasks. Colors from blue to yellow reflect increasing GCaMP6f signals. Light blue arrowheads indicate the first few trials when the animal smelled the odors. Dark blue arrowhead indicates the first few trials when the animal started to lick for water. In early sessions, odor 1 was delivered and associated with water reward. In late sessions, besides odor 1: water trials, in half of the trials, odor 2 was delivered and associated with an air puff with 50% probability or nothing (odor 2: air puff/omission trials).
- (F) Average responses of first ten trials taken from all the sessions. Quantification of the Z score showed significant neuronal responses to both odor 1 and odor 2 (**p < 0.0001 compared to baseline).
- (G) Comparison of odor 1 responses in early sessions and late sessions showed that the response to odor was high in early sessions and then diminished in late sessions (**p < 0.01).
- (H) Average responses across sessions show significant responses to odor 1 and water in CAR+ hemisphere compared to that of control hemisphere (**p < 0.0001).
- (I) Average responses across sessions show significant response to air puff (**p < 0.0001 compared to omission trials) in CAR+ hemisphere (**p < 0.0001 compared to control hemisphere). Dashed lines indicate the onset of odors at time 0 and the onset of water or air puff at time 2. Area of shading represents SEM; n values represent the number of trials; Mann-Whitney U test.

techniques (Grove and Marsh, 2011; Mateo et al., 2015; Schneider-Schaulies, 2000). Here we developed a strategy to overcome the limitations of CAV-2 viral tropism by leveraging existing knowledge of the molecular mechanisms for CAV-2 internalization and axonal transport. We demonstrated that this receptor complementation strategy enables tropism-free, high-efficiency retrograde delivery of a range of cargos for anatomical and functional studies.

Receptor Complementation as a General Strategy to Overcome Tropism

Cell-type-specific tropism represents a problem for all viral techniques to reveal the ground truth in connectivity. For instance, unmyelinated sensory neurons (which account for >40% of dorsal root ganglia neurons) are largely resistant to rabies virus infection from the spinal cord (Albisetti et al., 2017); HSV and CAV-2 infect different subpopulations of mPFC-projecting BLA neurons (Senn et al., 2014). A recent strategy to overcome tropism is to modify the viral surface structures. For example, lentivirus can be pseudotyped by replacing its natural envelope glycoproteins with heterologous envelope glycoproteins derived from other viruses (e.g., rabies virus glycoproteins or vesicular stomatitis virus glycoproteins) (Cetin and Callaway, 2014; Knowland et al., 2017; Cronin et al., 2005; Mazarakis et al., 2001). AAV capsids can be randomly mutated and screened for improved tropism or be engineered to include ligand motifs that can bind to surface receptors of certain cell types (Sallach et al., 2014; Wu et al., 2006). However, no matter which envelope or capsid is employed, viruses still rely on cell surface molecules for uptake and transport and cannot gain entry into cells without the required receptors.

The receptor complementation strategy we used here side steps viral tropism and expands the possibilities for future studies. Many viruses use just one or two molecules as receptors: the laminin receptor for the Sindbis virus (Wang et al., 1992), Nectin-1/2 or HVEM for HSV1/2 (Geraghty et al., 1998; Montgomery et al., 1996), CAR, and $\alpha\beta$ integrins for adenovirus-2 (Bergelson et al., 1997; Wickham et al., 1993). Even for diverse AAV serotypes, which had been believed to recognize distinct cell surface attachment and transport receptors, one universal AAV receptor critical for cellular entry and trafficking was recently identified (Pillay et al., 2016). Therefore, similar receptor complementation approaches applied to other neurotropic viruses may provide a valuable addition to the array of reagents for targeting and manipulating circuit-defined neuron types.

A Dual Virus Strategy with AAV-CAR and CAV-2 Is a Useful Tool for Retrograde Targeting

Classical retrograde tracers have provided essential tools for mapping long-range projections, including CTB (Luppi et al., 1990; Wan et al., 1982), the organic dye fluoro-gold (FG) (Schmued and Fallon, 1986), and latex microspheres (retro-beads) (Katz et al., 1984). Viral vectors provide important advantages over these tracers by permitting cell-type-specific promoters and flexible genetic cargo (Nassi et al., 2015; Ugolini, 2010). A number of different retrograde viruses have been used for projection-specific gene delivery, including the rabies virus, HSV, PRV, pseudotyped lentiviruses, capsid pseudotyped or engineered recombinant AAVs, and CAV-2. All of these viruses have

distinct advantages for neuroscience, with varying degrees of limitations on pathway tropisms, efficiency of retrograde transport, and cytotoxicity (Aston-Jones and Card, 2000; Ekstrand et al., 2008; Frampton et al., 2005; Luo et al., 2008; Murlidharan et al., 2014; Nassi et al., 2015; Ugolini, 2010). For instance, rabies virus can spread trans-synaptically, and its glycoprotein-deleted and EnvA pseudotyped variants enable identification of direct monosynaptic inputs to specific cell types (Callaway and Luo, 2015; Huang et al., 2013; Wall et al., 2010; Wertz et al., 2015; Wickersham et al., 2007). Notably, in this system, the expression of TVA receptor directs infection of the EnvA-pseudotyped rabies virus to defined cell types, which is another example of receptor complementation and engineered tropism. The toxicity of rabies virus, however, limits the time window for viable physiological experiments, although novel strains do exhibit significantly reduced toxicity (Chatterjee et al., 2018; Reardon et al., 2016; Schnell et al., 2010). In addition, as an RNA virus, rabies cannot be combined with the Cre-lox DNA recombination system.

The newly developed retrograde AAV variant rAAV2-retro is a particularly valuable reagent as a single-component labeling system that can be flexibly customized. Although tropism is rarely a concern for common AAVs due to the availability of numerous serotypes, the special retro-capsid that enables rAAV2-retro to undergo retrograde transport also restricts its tropism, limiting the usability of rAAV2-retro in some pathways (Tervo et al., 2016). Although the delivery of CAR relies on an AAV vector, the wide range of AAV serotypes available enables the targeting of most neuron types in question. In support of this, we observed much weaker labeling efficiency of rAAV2-retro relative to CAR/CAV-2 in dopaminergic VTA/SN neurons projecting to striatum (Figure 5). We also observed that, in addition to the expected axonal expression in striatum, Synaptophysin-mCherry had unexpected somatic expression at rAAV2-retro-Cre injection sites but not at CAV-Cre injection sites (Figure S4A). One possible reason for this abnormal pattern is because rAAV2-retro-Cre non-specifically infected the reciprocal projection striatum → VTA/SNc, where AAV8-DIO-[SYN-mCherry]_{on} may have weak retrograde transport back to the soma in the striatum that was turned on by rAAV2-retro-Cre. It is unclear whether rAAV2-retro enhances the retrograde transport of other AAVs when infecting the same neuron, but this possibility should be considered.

CAV-2 vectors have become widely used reagents for retrograde targeting in neuroscience largely due to their preferential transduction and retrograde transport in neurons and relatively low immunogenicity in the brains (Figure S4B) (Perreau and Kremer, 2005; Salinas et al., 2009; Soudais et al., 2001, 2004; Zussy et al., 2016). We used a dual virus strategy with Cre-recombinase-encoding CAV-2 in conjunction with Cre-dependent AAV vectors, a strategy that has become widespread (Beyeler et al., 2016; Burgos-Robles et al., 2017; Darvas and Palmiter, 2009; Kim et al., 2015; Nectow et al., 2015; Ruder et al., 2016; Senn et al., 2014; Wu et al., 2012). Although this dual virus injection strategy is more cumbersome compared to using a single retrograde virus, it also yields significant and unique advantages. First, it provides highly amplified labeling efficiency because even trace amounts of Cre recombinase are able to produce robust transgene expression. Second, the use of anterograde

AAV and retrograde CAV-Cre enables control over the direction or polarity of targeting: after retrograde transport of CAV-2 from distal axon terminals back to soma, the Cre recombinase expresses in the nucleus and activates the selective expression of AAV cargos only in neurons that project from the AAV injection site to the CAV-2 injection site. This dual virus strategy can be especially useful for reciprocal pathways as described above, as well as cargos such as DREADDs, whose activation is usually not spatially controlled (Boender et al., 2014; Carter et al., 2013). In contrast, in reciprocal pathways, a single retrograde virus will result in retrograde transport, as well as expression in the anterograde direction, because retrograde viruses can still infect neuronal cell bodies directly.

We have generated an assortment of vectors expressing CAR with different cargos useful for systems neuroscience (Table 1) and demonstrate their accurate and efficient targeting *in vivo* (Figures 2, 3, 4, 5, and 6). In addition, our CAR vector can also be used as a helper virus by simply mixing it with other AAVs, boosting the overall CAV-driven expression in AAV mixtures (Figures 4 and 5). For instance, AAV-CAR is expected to enhance the efficiency of more complex tracing strategies that employ CAV-2, such as TRIO (Schwarz et al., 2015).

CAR/CAV-2 Strategy Is Effective for *In Vivo*

Physiological Studies

A potential concern for the receptor potentiation approach is that overexpression of CAR might produce toxicity in neurons or, conversely, promote changes in neuronal morphology or wiring. A study in explant cultures from the retina indicated that CAR may be involved in adhesion and neurite extension in the developing nervous system (Patzke et al., 2010). In the brain, CAR is predominantly expressed during embryonic development, while expression drops rapidly after birth and varies across brain regions throughout adulthood (Honda et al., 2000; Zussy et al., 2016). However, the complete genetic deletion of CAR from a mouse brain resulted in no gross morphological anomalies, although it did cause a minor change in packing density and adult neurogenesis in hippocampal dentate gyrus (Zussy et al., 2016). Thus, the range of CAR phenotypes appear relatively minor and restricted largely to developmental periods that occur earlier than time points for CAV2 infection typically used in functional studies. In addition, our Cre-dependent strategy guarantees that CAR expression is turned off following retrograde infection by CAV-Cre in the neurons under study (Figure 3; Figure S2).

Overexpression of CAR, in our hands, did not result in obvious blebbing or filopodia in the cell body or in the elaboration of dendrites or changes in projection patterns of the infected neurons. The synaptic puncta density on axon fibers was identical between CAR-potentiated and control neurons, implying that the expression of CAR has no obvious impact on the strength of synaptic connection or the growth of neurites (Figure 4). In addition, TUNEL staining failed to detect any significant cellular apoptosis caused by CAV-2 (Figure S4B). Calcium imaging from behaving mice showed that CAR-potentiated neurons retained robust functional responses to multiple stimuli (Figure 6; Figure S5). These data demonstrate that the CAR/CAV-2 system overcomes viral tropisms and offers an enhanced retrograde targeting tool for linking connectivity to function in neural circuits.

STAR★METHODS

Detailed methods are provided in the online version of this paper and include the following:

- KEY RESOURCES TABLE
- CONTACT FOR REAGENT AND RESOURCE SHARING
- EXPERIMENTAL MODEL AND SUBJECT DETAILS
 - Animals
 - Primary Cell Cultures
- METHOD DETAILS
 - Recombinant AAV Cloning and Production
 - Stereotaxic Injections and Fiber Implantation
 - Animal Behavior Training and Fiber Photometry
 - Immunostaining, TUNEL Staining, and Immunoblotting
- QUANTIFICATION AND STATISTICAL ANALYSIS
- DATA AND SOFTWARE AVAILABILITY

SUPPLEMENTAL INFORMATION

Supplemental Information includes five figures and can be found with this article online at <https://doi.org/10.1016/j.neuron.2018.05.028>.

ACKNOWLEDGMENTS

This work was supported by grants from National Science Foundation (NSF) Early Concept Grants for Exploratory Research (EAGER) (1547967) and the National Institute of Health (U01 NS094288) (to A.K.), and NARSAD Young Investigator Award (26726) (to J.F.S.).

AUTHOR CONTRIBUTIONS

Conceptualization, S.-J.L., A.V., and A.K.; Methodology, S.-J.L. and A.K.; Investigation and Analysis of Anatomical Experiments, S.-J.L.; Investigation and Analysis of Calcium Imaging Experiments, S.-J.L. and J.F.S.; Writing – Original Draft, S.-J.L.; Writing – Review & Editing, S.-J.L., A.V., J.F.S., and A.K.; Supervision, A.K.

DECLARATION OF INTERESTS

The authors declare no competing interests.

Received: February 24, 2017

Revised: March 30, 2018

Accepted: May 17, 2018

Published: June 6, 2018

REFERENCES

- Albisetti, G.W., Ghanem, A., Foster, E., Conzelmann, K.-K., Zeilhofer, H.U., and Wildner, H. (2017). Identification of two classes of somatosensory neurons that display resistance to retrograde infection by rabies virus. *J. Neurosci.* 37, 10358–10371.
- Aston-Jones, G., and Card, J.P. (2000). Use of pseudorabies virus to delineate multisynaptic circuits in brain: opportunities and limitations. *J. Neurosci. Methods* 103, 51–61.
- Atasoy, D., Aponte, Y., Su, H.H., and Sternson, S.M. (2008). A FLEX switch targets Channelrhodopsin-2 to multiple cell types for imaging and long-range circuit mapping. *J. Neurosci.* 28, 7025–7030.
- Bergelson, J.M., Cunningham, J.A., Drogue, G., Kurt-Jones, E.A., Krishnas, A., Hong, J.S., Horwitz, M.S., Crowell, R.L., and Finberg, R.W. (1997). Isolation of a common receptor for Coxsackie B viruses and adenoviruses 2 and 5. *Science* 275, 1320–1323.

- Bergelson, J.M., Krishnaswamy, A., Celi, L., Drogouet, G., Horwitz, M.S., Wickham, T., Crowell, R.L., and Finberg, R.W. (1998). The murine CAR homolog is a receptor for coxsackie B viruses and adenoviruses. *J. Virol.* 72, 415–419.
- Beyeler, A., Namburi, P., Glober, G.F., Simonnet, C., Calhoun, G.G., Conyers, G.F., Luck, R., Wildes, C.P., and Tye, K.M. (2016). Divergent routing of positive and negative information from the amygdala during memory retrieval. *Neuron* 90, 348–361.
- Boender, A.J., de Jong, J.W., Boekhoudt, L., Luijendijk, M.C., van der Plasse, G., and Adan, R.A. (2014). Combined use of the canine adenovirus-2 and DREADD-technology to activate specific neural pathways in vivo. *PLoS ONE* 9, e95392.
- Boldogkoi, Z., Balint, K., Awatramani, G.B., Balya, D., Busskamp, V., Viney, T.J., Lagali, P.S., Duebel, J., Pásti, E., Tombácz, D., et al. (2009). Genetically timed, activity-sensor and rainbow transsynaptic viral tools. *Nat. Methods* 6, 127–130.
- Burgos-Robles, A., Kimchi, E.Y., Izadmehr, E.M., Porzenheim, M.J., Ramos-Guasp, W.A., Nieh, E.H., Felix-Ortiz, A.C., Namburi, P., Leppla, C.A., Presbrey, K.N., et al. (2017). Amygdala inputs to prefrontal cortex guide behavior amid conflicting cues of reward and punishment. *Nat. Neurosci.* 20, 824–835.
- Callaway, E.M., and Luo, L. (2015). Monosynaptic circuit tracing with glycoprotein-deleted rabies viruses. *J. Neurosci.* 35, 8979–8985.
- Cambridge, S.B., Gnad, F., Nguyen, C., Bermejo, J.L., Krüger, M., and Mann, M. (2011). Systems-wide proteomic analysis in mammalian cells reveals conserved, functional protein turnover. *J. Proteome Res.* 10, 5275–5284.
- Carter, M.E., Soden, M.E., Zweifel, L.S., and Palmiter, R.D. (2013). Genetic identification of a neural circuit that suppresses appetite. *Nature* 503, 111–114.
- Cetin, A., and Callaway, E.M. (2014). Optical control of retrogradely infected neurons using drug-regulated “TLoop” lentiviral vectors. *J. Neurophysiol.* 111, 2150–2159.
- Chatterjee, S., Sullivan, H.A., MacLennan, B.J., Xu, R., Hou, Y., Lavin, T.K., Lea, N.E., Michalski, J.E., Babcock, K.R., Dietrich, S., et al. (2018). Nontoxic, double-deletion-mutant rabies viral vectors for retrograde targeting of projection neurons. *Nat. Neurosci.* 21, 638–646.
- Chen, T.W., Wardill, T.J., Sun, Y., Pulver, S.R., Renninger, S.L., Baohan, A., Schreiter, E.R., Kerr, R.A., Orger, M.B., Jayaraman, V., et al. (2013). Ultrasensitive fluorescent proteins for imaging neuronal activity. *Nature* 499, 295–300.
- Choi, J.H., Yu, N.K., Baek, G.C., Bakes, J., Seo, D., Nam, H.J., Baek, S.H., Lim, C.S., Lee, Y.S., and Kaang, B.K. (2014). Optimization of AAV expression cassettes to improve packaging capacity and transgene expression in neurons. *Mol. Brain* 7, 17.
- Cronin, J., Zhang, X.Y., and Reiser, J. (2005). Altering the tropism of lentiviral vectors through pseudotyping. *Curr. Gene Ther.* 5, 387–398.
- Cui, G., Jun, S.B., Jin, X., Pham, M.D., Vogel, S.S., Lovering, D.M., and Costa, R.M. (2013). Concurrent activation of striatal direct and indirect pathways during action initiation. *Nature* 494, 238–242.
- Darvas, M., and Palmiter, R.D. (2009). Restriction of dopamine signaling to the dorsolateral striatum is sufficient for many cognitive behaviors. *Proc. Natl. Acad. Sci. USA* 106, 14664–14669.
- Ekstrand, M.I., Enquist, L.W., and Pomeranz, L.E. (2008). The alpha-herpesviruses: molecular pathfinders in nervous system circuits. *Trends Mol. Med.* 14, 134–140.
- Ekstrand, M.I., Nectow, A.R., Knight, Z.A., Latcha, K.N., Pomeranz, L.E., and Friedman, J.M. (2014). Molecular profiling of neurons based on connectivity. *Cell* 157, 1230–1242.
- Frampton, A.R., Jr., Goins, W.F., Nakano, K., Burton, E.A., and Glorioso, J.C. (2005). HSV trafficking and development of gene therapy vectors with applications in the nervous system. *Gene Ther.* 12, 891–901.
- Garfield, A.S., Shah, B.P., Madara, J.C., Burke, L.K., Patterson, C.M., Flak, J., Neve, R.L., Evans, M.L., Lowell, B.B., Myers, M.G., Jr., and Heisler, L.K. (2014). A parabrachial-hypothalamic cholecystokinin neurocircuit controls counterregulatory responses to hypoglycemia. *Cell Metab.* 20, 1030–1037.
- Geraghty, R.J., Krummenacher, C., Cohen, G.H., Eisenberg, R.J., and Spear, P.G. (1998). Entry of alphaherpesviruses mediated by poliovirus receptor-related protein 1 and poliovirus receptor. *Science* 280, 1618–1620.
- Grove, J., and Marsh, M. (2011). The cell biology of receptor-mediated virus entry. *J. Cell Biol.* 195, 1071–1082.
- Gunaydin, L.A., Yizhar, O., Berndt, A., Sohal, V.S., Deisseroth, K., and Hegemann, P. (2010). Ultrafast optogenetic control. *Nat. Neurosci.* 13, 387–392.
- Henaff, D., and Salinas, S. (2010). An endocytic CARriage tale: adenoviruses internalization and trafficking in neurons. *Virulence* 1, 188–191.
- Hnasko, T.S., Perez, F.A., Scouras, A.D., Stoll, E.A., Gale, S.D., Luquet, S., Phillips, P.E., Kremer, E.J., and Palmiter, R.D. (2006). Cre recombinase-mediated restoration of nigrostriatal dopamine in dopamine-deficient mice reverses hypophagia and bradykinesia. *Proc. Natl. Acad. Sci. USA* 103, 8858–8863.
- Honda, T., Saitoh, H., Masuko, M., Katagiri-Abe, T., Tominaga, K., Kozakai, I., Kobayashi, K., Kumanishi, T., Watanabe, Y.G., Odani, S., and Kuwano, R. (2000). The coxsackievirus-adenovirus receptor protein as a cell adhesion molecule in the developing mouse brain. *Brain Res. Mol. Brain Res.* 77, 19–28.
- Huang, C.C., Sugino, K., Shima, Y., Guo, C., Bai, S., Mensh, B.D., Nelson, S.B., and Hantman, A.W. (2013). Convergence of pontine and proprioceptive streams onto multimodal cerebellar granule cells. *eLife* 2, e00400.
- Janak, P.H., and Tye, K.M. (2015). From circuits to behaviour in the amygdala. *Nature* 517, 284–292.
- Junyent, F., and Kremer, E.J. (2015). CAV-2—why a canine virus is a neurobiologist's best friend. *Curr. Opin. Pharmacol.* 24, 86–93.
- Katz, L.C., Burkhalter, A., and Dreyer, W.J. (1984). Fluorescent latex microspheres as a retrograde neuronal marker for in vivo and in vitro studies of visual cortex. *Nature* 310, 498–500.
- Kim, E.J., Juavinett, A.L., Kyubwa, E.M., Jacobs, M.W., and Callaway, E.M. (2015). Three types of cortical layer 5 neurons that differ in brain-wide connectivity and function. *Neuron* 88, 1253–1267.
- Knowland, D., Lilascharoen, V., Pacia, C.P., Shin, S., Wang, E.H.-J., and Lim, B.K. (2017). Distinct ventral pallidal neural populations mediate separate symptoms of depression. *Cell* 170, 284–297.e18.
- Kügler, S., Kilic, E., and Bähr, M. (2003). Human synapsin 1 gene promoter confers highly neuron-specific long-term transgene expression from an adenoviral vector in the adult rat brain depending on the transduced area. *Gene Ther.* 10, 337–347.
- Lerner, T.N., Shilyansky, C., Davidson, T.J., Evans, K.E., Beier, K.T., Zalocusky, K.A., Crow, A.K., Malenka, R.C., Luo, L., Tomer, R., and Deisseroth, K. (2015). Intact-brain analyses reveal distinct information carried by SNc dopamine subcircuits. *Cell* 162, 635–647.
- Lilley, C.E., Groutsis, F., Han, Z., Palmer, J.A., Anderson, P.N., Latchman, D.S., and Coffin, R.S. (2001). Multiple immediate-early gene-deficient herpes simplex virus vectors allowing efficient gene delivery to neurons in culture and widespread gene delivery to the central nervous system in vivo. *J. Virol.* 75, 4343–4356.
- Luo, L., Callaway, E.M., and Svoboda, K. (2008). Genetic dissection of neural circuits. *Neuron* 57, 634–660.
- Luppi, P.H., Fort, P., and Jouvet, M. (1990). Iontophoretic application of unconjugated cholera toxin B subunit (CTB) combined with immunohistochemistry of neurochemical substances: a method for transmitter identification of retrogradely labeled neurons. *Brain Res.* 534, 209–224.
- Maren, S., and Quirk, G.J. (2004). Neuronal signalling of fear memory. *Nat. Rev. Neurosci.* 5, 844–852.
- Mateo, M., Generous, A., Sinn, P.L., and Cattaneo, R. (2015). Connections matter—how viruses use cell-cell adhesion components. *J. Cell Sci.* 128, 431–439.
- Mazarakis, N.D., Azzouz, M., Rohll, J.B., Ellard, F.M., Wilkes, F.J., Olsen, A.L., Carter, E.E., Barber, R.D., Baban, D.F., Kingsman, S.M., et al. (2001). Rabies virus glycoprotein pseudotyping of lentiviral vectors enables retrograde axonal transport and access to the nervous system after peripheral delivery. *Hum. Mol. Genet.* 10, 2109–2121.
- Miyamichi, K., Shlomai-Fuchs, Y., Shu, M., Weissbourd, B.C., Luo, L., and Mizrahi, A. (2013). Dissecting local circuits: parvalbumin interneurons underlie broad feedback control of olfactory bulb output. *Neuron* 80, 1232–1245.
- Montgomery, R.I., Warner, M.S., Lum, B.J., and Spear, P.G. (1996). Herpes simplex virus-1 entry into cells mediated by a novel member of the TNF/NGF receptor family. *Cell* 87, 427–436.

- Murlidharan, G., Samulski, R.J., and Asokan, A. (2014). Biology of adeno-associated viral vectors in the central nervous system. *Front. Mol. Neurosci.* 7, 76.
- Nassi, J.J., Cepko, C.L., Born, R.T., and Beier, K.T. (2015). Neuroanatomy goes viral! *Front. Neuroanat.* 9, 80.
- Nectow, A.R., Ekstrand, M.I., and Friedman, J.M. (2015). Molecular characterization of neuronal cell types based on patterns of projection with Retro-TRAP. *Nat. Protoc.* 10, 1319–1327.
- Oyibo, H.K., Znamenskiy, P., Oviedo, H.V., Enquist, L.W., and Zador, A.M. (2014). Long-term Cre-mediated retrograde tagging of neurons using a novel recombinant pseudorabies virus. *Front. Neuroanat.* 8, 86.
- Patzke, C., Max, K.E., Behlke, J., Schreiber, J., Schmidt, H., Dorner, A.A., Kröger, S., Henning, M., Otto, A., Heinemann, U., and Rathjen, F.G. (2010). The coxsackievirus-adenovirus receptor reveals complex homophilic and heterophilic interactions on neural cells. *J. Neurosci.* 30, 2897–2910.
- Perreau, M., and Kremer, E.J. (2005). Frequency, proliferation, and activation of human memory T cells induced by a nonhuman adenovirus. *J. Virol.* 79, 14595–14605.
- Pillay, S., Meyer, N.L., Puschnik, A.S., Davulcu, O., Diep, J., Ishikawa, Y., Jae, L.T., Wosen, J.E., Nagamine, C.M., Chapman, M.S., and Carette, J.E. (2016). An essential receptor for adeno-associated virus infection. *Nature* 530, 108–112.
- Reardon, T.R., Murray, A.J., Turi, G.F., Wirblich, C., Croce, K.R., Schnell, M.J., Jessell, T.M., and Losonczy, A. (2016). Rabies virus CVS-N2c(ΔG) strain enhances retrograde synaptic transfer and neuronal viability. *Neuron* 89, 711–724.
- Rogan, M.T., Stäubli, U.V., and LeDoux, J.E. (1997). Fear conditioning induces associative long-term potentiation in the amygdala. *Nature* 390, 604–607.
- Ruder, L., Takeoka, A., and Arber, S. (2016). Long-distance descending spinal neurons ensure quadrupedal locomotor stability. *Neuron* 92, 1063–1078.
- Saito, M., Iwawaki, T., Taya, C., Yonekawa, H., Noda, M., Inui, Y., Mekada, E., Kimata, Y., Tsuru, A., and Kohno, K. (2001). Diphtheria toxin receptor-mediated conditional and targeted cell ablation in transgenic mice. *Nat. Biotechnol.* 19, 746–750.
- Salinas, S., Bilsland, L.G., Henaff, D., Weston, A.E., Keriel, A., Schiavo, G., and Kremer, E.J. (2009). CAR-associated vesicular transport of an adenovirus in motor neuron axons. *PLoS Pathog.* 5, e1000442.
- Salinas, S., Zussy, C., Loustalot, F., Henaff, D., Menendez, G., Morton, P.E., Parsons, M., Schiavo, G., and Kremer, E.J. (2014). Disruption of the coxsackievirus and adenovirus receptor-homodimeric interaction triggers lipid micro-domain- and dynamin-dependent endocytosis and lysosomal targeting. *J. Biol. Chem.* 289, 680–695.
- Sallach, J., Di Pasquale, G., Larcher, F., Niehoff, N., Rübsam, M., Huber, A., Chiorini, J., Almarza, D., Eming, S.A., Ulus, H., et al. (2014). Tropism-modified AAV vectors overcome barriers to successful cutaneous therapy. *Mol. Ther.* 22, 929–939.
- Schmued, L.C., and Fallon, J.H. (1986). Fluoro-Gold: a new fluorescent retrograde axonal tracer with numerous unique properties. *Brain Res.* 377, 147–154.
- Schneider-Schaulies, J. (2000). Cellular receptors for viruses: links to tropism and pathogenesis. *J. Gen. Virol.* 81, 1413–1429.
- Schnell, M.J., McGettigan, J.P., Wirblich, C., and Papaneri, A. (2010). The cell biology of rabies virus: using stealth to reach the brain. *Nat. Rev. Microbiol.* 8, 51–61.
- Schnütgen, F., Doerflinger, N., Calléja, C., Wendling, O., Champon, P., and Ghyselinck, N.B. (2003). A directional strategy for monitoring Cre-mediated recombination at the cellular level in the mouse. *Nat. Biotechnol.* 21, 562–565.
- Schoenbaum, G., Chiba, A.A., and Gallagher, M. (1999). Neural encoding in orbitofrontal cortex and basolateral amygdala during olfactory discrimination learning. *J. Neurosci.* 19, 1876–1884.
- Schwarz, L.A., Miyamichi, K., Gao, X.J., Beier, K.T., Weissbourd, B., DeLoach, K.E., Ren, J., Ibanes, S., Malenka, R.C., Kremer, E.J., and Luo, L. (2015). Viral-genetic tracing of the input-output organization of a central noradrenaline circuit. *Nature* 524, 88–92.
- Senn, V., Wolff, S.B., Henry, C., Grenier, F., Ehrlich, I., Gründemann, J., Fadok, J.P., Müller, C., Letzkus, J.J., and Lüthi, A. (2014). Long-range connectivity defines behavioral specificity of amygdala neurons. *Neuron* 81, 428–437.
- Shabel, S.J., and Janak, P.H. (2009). Substantial similarity in amygdala neuronal activity during conditioned appetitive and aversive emotional arousal. *Proc. Natl. Acad. Sci. USA* 106, 15031–15036.
- Soudais, C., Boutin, S., Hong, S.S., Chillon, M., Danos, O., Bergelson, J.M., Boulanger, P., and Kremer, E.J. (2000). Canine adenovirus type 2 attachment and internalization: coxsackievirus-adenovirus receptor, alternative receptors, and an RGD-independent pathway. *J. Virol.* 74, 10639–10649.
- Soudais, C., Laplace-Builhe, C., Kiss, K., and Kremer, E.J. (2001). Preferential transduction of neurons by canine adenovirus vectors and their efficient retrograde transport in vivo. *FASEB J.* 15, 2283–2285.
- Soudais, C., Skander, N., and Kremer, E.J. (2004). Long-term in vivo transduction of neurons throughout the rat CNS using novel helper-dependent CAV-2 vectors. *FASEB J.* 18, 391–393.
- Takahashi, L.K., Nakashima, B.R., Hong, H., and Watanabe, K. (2005). The smell of danger: a behavioral and neural analysis of predator odor-induced fear. *Neurosci. Biobehav. Rev.* 29, 1157–1167.
- Tervo, D.G., Hwang, B.Y., Viswanathan, S., Gaj, T., Lavzin, M., Ritola, K.D., Lindo, S., Michael, S., Kuleshova, E., Ojala, D., et al. (2016). A designer AAV variant permits efficient retrograde access to projection neurons. *Neuron* 92, 372–382.
- Ugolini, G. (1995). Specificity of rabies virus as a transneuronal tracer of motor networks: transfer from hypoglossal motoneurons to connected second-order and higher order central nervous system cell groups. *J. Comp. Neurol.* 356, 457–480.
- Ugolini, G. (2010). Advances in viral transneuronal tracing. *J. Neurosci. Methods* 194, 2–20.
- Ugolini, G., Kuypers, H.G., and Simmons, A. (1987). Retrograde transneuronal transfer of herpes simplex virus type 1 (HSV 1) from motoneurones. *Brain Res.* 422, 242–256.
- Wall, N.R., Wickersham, I.R., Cetin, A., De La Parra, M., and Callaway, E.M. (2010). Monosynaptic circuit tracing in vivo through Cre-dependent targeting and complementation of modified rabies virus. *Proc. Natl. Acad. Sci. USA* 107, 21848–21853.
- Wan, X.C., Trojanowski, J.Q., and Gonatas, J.O. (1982). Cholera toxin and wheat germ agglutinin conjugates as neuroanatomical probes: their uptake and clearance, transganglionic and retrograde transport and sensitivity. *Brain Res.* 243, 215–224.
- Wang, K.S., Kuhn, R.J., Strauss, E.G., Ou, S., and Strauss, J.H. (1992). High-affinity laminin receptor is a receptor for Sindbis virus in mammalian cells. *J. Virol.* 66, 4992–5001.
- Wertz, A., Trenholm, S., Yonehara, K., Hillier, D., Raics, Z., Leinweber, M., Szalay, G., Ghanem, A., Keller, G., Rózsa, B., et al. (2015). PRESYNAPTIC NETWORKS. Single-cell-initiated monosynaptic tracing reveals layer-specific cortical network modules. *Science* 349, 70–74.
- Wickersham, I.R., Lyon, D.C., Barnard, R.J., Mori, T., Finke, S., Conzelmann, K.K., Young, J.A., and Callaway, E.M. (2007). Monosynaptic restriction of transsynaptic tracing from single, genetically targeted neurons. *Neuron* 53, 639–647.
- Wickham, T.J., Mathias, P., Cheresh, D.A., and Nemerow, G.R. (1993). Integrins alpha v beta 3 and alpha v beta 5 promote adenovirus internalization but not virus attachment. *Cell* 73, 309–319.
- Wu, Z., Asokan, A., and Samulski, R.J. (2006). Adeno-associated virus serotypes: vector toolkit for human gene therapy. *Mol. Ther.* 14, 316–327.
- Wu, Q., Clark, M.S., and Palmiter, R.D. (2012). Deciphering a neuronal circuit that mediates appetite. *Nature* 483, 594–597.
- Zussy, C., Loustalot, F., Junyent, F., Gardoni, F., Bories, C., Valero, J., Desarmenien, M.G., Bernex, F., Henaff, D., Bayo-Puxan, N., et al. (2016). Coxsackievirus adenovirus receptor loss impairs adult neurogenesis, synapse content, and hippocampus plasticity. *J. Neurosci.* 36, 9558–9571.

STAR★METHODS

KEY RESOURCES TABLE

REAGENT or RESOURCE	SOURCE	IDENTIFIER
Antibodies		
Goat polyclonal anti-HA	Abcam	Cat# ab9134; RRID: AB_307035
Mouse monoclonal anti-HA	Abcam	Cat# ab18181; RRID: AB_444303
Rabbit anti-RFP	Rockland	Cat# 600-401-379; RRID: AB_2209751
Rabbit anti-GFP Alexa Fluor 488-conjugated	Molecular Probes	Cat# A-21311; RRID: AB_221477
Mouse anti-GFP	Santa Cruz Biotechnology	Cat# sc-9996; RRID: AB_627695
Mouse anti-Myc 9E10	Santa Cruz Biotechnology	Cat# sc-40; RRID: AB_627268
Rabbit anti-Cre	Millipore	Cat# 69050-3; RRID: AB_10806983
Rabbit anti-mCherry	Abcam	Cat# ab167453; RRID: AB_2571870
Chicken anti-mCherry	Novus	Cat# NBP2-25158; RRID: AB_2636881
Chicken anti-TH	Abcam	Cat# ab76442; RRID: AB_1524535
Rabbit anti-Tubulin	Abcam	Cat# ab179512
Bacterial and Virus Strains		
AAV9-DIO-{ChrR2}on	This paper	N/A
AAV9-DIO-{mCAR}off{ChrR2}on	This paper	N/A
AAV9-DIO-{ChrR2-mRuby2}on-W3SL	This paper	N/A
AAV9-DIO-{hCAR}off{ChrR2-mRuby2}on-W3SL	This paper	N/A
AAV9-DIO-{hCAR}off{GCaMP6f}on-W3SL	This paper	N/A
AAV8-Ef1a-DIO-{Synaptophysin-mCherry}on	MIT Viral Gene Transfer Core	N/A
AAV9-hSyn-Flex-GCaMP6f-WPRE-SV40	Penn Vector Core	N/A
CAV-Cre	Montpellier vectorology platform	N/A
CAV-dsRed	Montpellier vectorology platform	N/A
CAV-CreGFP	Montpellier vectorology platform	N/A
rAAV2-retro-Syn-Cre	Janelia Research Campus Virus Services	N/A
Chemicals, Peptides, and Recombinant Proteins		
Cholera toxin subunit B-647	Thermo Fisher Scientific	C34778
red retrobeads	Lumafluor	Cat# R170
Glycerol Mounting Medium With DAPI and DABCO	Electron Microscopy Sciences	Cat# 17989-61
Critical Commercial Assays		
TUNEL assay kit	Roche	Cat# 11684795910
Experimental Models: Cell Lines		
Mouse: primary hippocampal neurons	This paper	N/A
Experimental Models: Organisms/Strains		
Mouse: C57BL/6	Charles River	RRID: IMSR_JAX:000664
Rat: Long Evans	Charles River	RRID: RGD_2308852
Recombinant DNA		
pAAV-DIO-{ChrR2}on	This paper	Addgene, Plasmid Cat# 111386
pAAV-DIO-{mCAR}off{ChrR2}on	This paper	Addgene, Plasmid Cat# 111387
pAAV-DIO-{hCAR}off{ChrR2}on	This paper	Addgene, Plasmid Cat# 111388
pAAV-DIO-{ChrR2-mRuby2}on-W3SL	This paper	Addgene, Plasmid Cat# 111389
pAAV-DIO-{mCAR}off{ChrR2-mRuby2}on-W3SL	This paper	Addgene, Plasmid Cat# 111390

(Continued on next page)

Continued

REAGENT or RESOURCE	SOURCE	IDENTIFIER
pAAV-DIO-{hCAR}off{ChR2-mRuby2}on-W3SL	This paper	Addgene, Plasmid Cat# 111391
pAAV-DIO-{hCAR}off{ChR2-EYFP}on-W3SL	This paper	Addgene, Plasmid Cat# 111392
pAAV-DIO-{mCAR}off{GCaMP6f}on	This paper	Addgene, Plasmid Cat# 111393
pAAV-DIO-{hCAR}off{GCaMP6f}on-W3SL	This paper	Addgene, Plasmid Cat# 111394
pAAV-DIO-{mCAR}off{DTR-GFP}on	This paper	Addgene, Plasmid Cat# 111395
pAAV-DIO-{hCAR}off{DTR-GFP}on-W3SL	This paper	Addgene, Plasmid Cat# 111396
pAAV-DIO-{hCAR}off{hM4Di-mCherry}on-W3SL	This paper	Addgene, Plasmid Cat# 111397
pAAV-Ef1a-DIO-{ChETA-EYFP}	Karl Deisseroth Lab; Gunaydin et al., 2010	Addgene, Plasmid #26968
Mouse <i>Car</i> variant 2	Dharmacon	Accession: BC016457; Clone ID: 4216727
Human <i>CAR</i> variant 1	Dharmacon	Accession: BC010536; Clone ID: 3456544
W3SL	Bong-Kiun Kaang Lab; Choi et al., 2014	Addgene, Plasmid #61463
hM4Di-mCherry	Bryan Roth Lab	Addgene, Plasmid #50461
Software and Algorithms		
Image-Pro Plus	Media Cybernetics	RRID: SCR_007369; http://www.mediacy.com/imageproplus
GraphPad Prism	GraphPad	RRID: SCR_002798; https://www.graphpad.com/scientific-software/prism/
MATLAB	MathWorks	RRID: SCR_001622; https://www.mathworks.com/pricing-licensing.html?prodcode=ML
ImageJ	NIH	RRID: SCR_003070; https://imagej.nih.gov/ij/
Other		
Bpod State Machine	Adam Kepcs and Joshua Sanders (SanWorks)	https://sites.google.com/site/bpoddocumentation/

CONTACT FOR REAGENT AND RESOURCE SHARING

Further information and requests for resources and reagents should be directed to and will be fulfilled by the Lead Contact, Adam Kepcs (kepecs@cshl.edu).

EXPERIMENTAL MODEL AND SUBJECT DETAILS**Animals**

Adult C57BL/6 mice (over 2 months old, females and males, Charles River, RRID: IMSR_JAX:000664) and adult Long Evans rats (over 10 weeks old, males only, Charles River, RRID: RGD_2308852) were used under the protocol approved by Cold Spring Harbor Laboratory Institutional Animal Care and Use Committee in accordance with National Institutes of Health regulations.

Primary Cell Cultures

The primary hippocampal neuronal cultures were prepared from P0 C57BL/6 female or male mouse pups and were plated on 6 well-plate (Falcon) in medium consisting of Neurobasal medium (Invitrogen), B-27 (Invitrogen) and 2 mM Glutamax-I (Invitrogen) at 37°C in a humidified incubator with 5% CO₂/air.

METHOD DETAILS**Recombinant AAV Cloning and Production**

The backbone of vector hSyn-DIO-WPRE was based on pAAV-Ef1a-DIO-{ChETA-EYFP} vector from Deisseroth Lab (Addgene, Plasmid #26968) except the Ef1a promoter was replaced with the human synapsin 1 gene promoter. In the hSyn-DIO-W3SL vector, the WPRE and bGH polyadenylation cassettes were replaced by W3SL cassette. All transgenes were amplified from existing vectors: mouse *Car* variant 2 (GenBank: NM_009988, 162-1217 nt, Dharmacon Accession: BC016457, Clone ID: 4216727), human *CAR* variant 1 (GenBank: NM_001338, 225-1319 nt, Dharmacon Accession: BC010536, Clone ID: 3456544), ChETA (Addgene, Plasmid #26968, a gift from Karl Deisseroth) ([Gunaydin et al., 2010](#)), W3SL (Addgene, Plasmid #61463, a gift from Bong-Kiun Kaang) ([Choi](#)

[et al., 2014](#)), hM4Di-mCherry (Addgene, Plasmid #50461, a gift from Bryan Roth), mRuby2 (from construct AAV-Ef1a-DIO-mRuby2, a gift from A.M. Zador, Cold Spring Harbor Laboratory), GCaMP6f and DTR-GFP (original constructs are gifts from D.F. Albeanu, Cold Spring Harbor Laboratory).

The coding sequences of mCAR and hCAR were fused with Myc tag, and located next to the promoter and first pair of incompatible lox sites (loxP and lox2722) in sense orientation. ChETA were fused with either HA tag or mRuby2 fluorescent protein, and positioned next to the second pair of lox sites in antisense orientation. A short motif including stop codons and PacI site (TAATTAATTAATTAA) were used as a linker. All vectors were amplified with recombination deficient bacteria (OneShot Stbl3, Invitrogen). Functional vectors were packaged as serotype 9 by a commercial vector core facility (University of North Carolina). The titers for each virus are shown below: AAV-DIO-[ChR2]_{on} 5.2E12 vg/ml; AAV-DIO-[mCAR]_{off}[ChR2]_{on} 5.0E12 vg/ml; AAV-DIO-[ChR2-mRuby2]_{on}-W3SL 7.8E12 vg/ml; AAV-DIO-[hCAR]_{off}[ChR2-mRuby2]_{on}-W3SL 4.5E12 vg/ml; AAV9-hSyn-DIO-[hCAR]_{off}[GCaMP6f]_{on}-W3SL 7.6E12 vg/ml. The titers for commercially available viruses are shown below: AAV8-Ef1a-DIO-[Synaptophysin-mCherry]_{on} 1.3E13 vg/ml (MIT Viral Gene Transfer Core); AAV9-hSyn-Flex-GCaMP6f-WPRE-SV40 7.76E12 GC/ml (Penn Vector Core); CAV-Cre 4.1E12 pp/ml, CAV-dsRed 5.7E12 pp/ml, CAV-CreGFP 5.4E12 pp/ml (Montpellier vectorology platform), rAAV2-retro-Syn-Cre 4.7E12 GC/ml (Gift from Janelia Research Campus Virus Services).

Stereotaxic Injections and Fiber Implantation

Animals were anaesthetized with a mixture of ketamine (125 mg/kg) and xylazine (10 mg/kg) administered intraperitoneally after a brief induction with isoflurane. Surgical anesthesia was maintained with supplementary doses of ketamine/xylazine and isoflurane as necessary. The skin and connective tissues of the scalp were injected with lidocaine subcutaneously; eyes were protected with ophthalmic lubricant (Puralube Vet Ointment, Dechra Pharmaceuticals Plc.). Mice were placed in a stereotax (David Kopf Instruments) and the skull was leveled along both the antero-posterior and medio-lateral axis to allow precise targeting. Cranial windows were opened above the target coordinates: mouse BLA viral injections (AP: -1.2 mm, ML: 3.0 mm, DV: 4.5 and 4.2 mm from brain surface), BLA fiber implantations (AP: -1.2 mm, ML: 3.3 mm, DV: 4.2 mm), mPFC (AP: +1.9 mm, ML: 0.4 mm, DV: 2.0 and 1.4 mm), VTA/SNC (AP: -2.9 mm, ML: 0.8 mm, DV: 4.5 and 4.0 mm), DLS (AP: +0.6 mm, ML: 2.25 mm, DV: 2.8 and 2.5 mm), rat vCA1 (AP: -5.0 mm, ML: 5.3 mm, DV: 6.5, 6.2 and 5.9 mm), rat mPFC (AP: +2.4 mm, ML: 0.5 mm, DV: 3.0 and 2.5 mm), rat OFC (AP: +3.7 mm, ML: 3.2 mm, DV: 3.0 and 2.7 mm), rat VS (AP: +1.2 mm, ML: 2.3 mm, DV: 6.3 and 6.0 mm). At each dorso-ventral level, 150 nL virus was injected slowly for 4 mins via a glass pipette pulled (P-97 Flaming/Brown Micropipette Puller, Sutter Instruments) from borosilicate capillaries (5 μ L; tip diameter 20 μ m). After injections, the pipette was slowly pulled out after a 5-minutes' waiting time. Then the craniotomies were covered by low viscosity silicone elastomer sealant (Kwik-Cast, World Precision Instruments). Suture and tissue adhesive (3M Vetbond) were applied to close the wound. Then animals received a subcutaneous injection of analgesic solution (Ketoprofen, 5 mg/kg). Three days' postoperative monitoring period were applied during the recovery of animals.

For the mouse BLA → mPFC projection, CAR-expressing AAVs and corresponding control AAVs were randomly injected into BLA in opposing hemispheres on the same day. After 7-9 days, a 1:1 mixture of CAV-CreGFP and CTB (Thermo Fisher Scientific, C34778, Alexa Fluor 647 Conjugate, 1 mg/ml) or a 1:1:2 mixture of CAV-dsRed/CAV-Cre/CTB was made and injected into both hemispheres of mPFC with same volumes. Animals were sacrificed 9-12 days after CAV-2 injections.

For rat pathways the same strategy was applied, except that the waiting time for post-infection was generally longer in consideration of bigger brain size and longer axonal traveling distance. For vCA1 → mPFC projection, a 1:1 mixture of CAV-CreGFP and red retrobeads (Lumafluor) was made; the post-infection last for 14-30 days after AAV injections, 14-40 days after CAV-2 injections. For rat OFC → VS projection, a 1:1 mixture of reporter virus AAV8-Ef1a-DIO-[Synaptophysin-mCherry]_{on} with CAR expressing virus AAV-DIO-[mCAR]_{off}[ChR2]_{on} or control virus AAV-DIO-[ChR2]_{on} were made and injected into opposing OFC; After 8-9 days, a 1:1 mixture of CAV-CreGFP and CTB was made and injected into VS on opposing hemisphere with same volume; Animals were sacrificed 14-24 days after CAV-2 injections.

For comparison of CAR/CAV-2 and rAAV2-retro infectivity in VTA/SNC-DLS pathway, a 1:1 mixture of the reporter virus AAV8-Ef1a-DIO-[Synaptophysin-mCherry]_{on} with CAR-expressing virus AAV-DIO-[mCAR]_{off}[ChR2]_{on} was made and injected in opposing VTAs. After 1-3 weeks (results with different post-infection time were similar thus combined together), CTB was 1:1 mixed with CAV-Cre or rAAV2-retro-Cre respectively and injected into opposing DLS with same titer and volume. Animals were sacrificed 9-15 days later.

For investigating the optimal timing of AAV and CAV-2 injections, in CAR+ versus Control group, the AAV and CAV-2 injections were on the same day (0 dbi), and the post-infection last for 9-14 days. For the no delay (0 dbi) versus seven day 7 delay (7 dbi) groups, two animals received CAR-expressing AAV injections in both left and right BLA, as well as CAV-2 injection in mPFC on one hemisphere on Day 0, then received the second CAV-2 injection with same volume in contralateral mPFC on Day 7; one animal received CAR-expressing AAV injection in one side of BLA on Day 0, then received the second AAV injection with same volume in contralateral BLA as well as CAV-2 injections in both hemispheres of mPFC on Day 7; animals were sacrificed 8-11 days after the final CAV-2 injections. The results for these three animals were similar and thus combined together. For 3 dbi versus 7 dbi, 7 dbi versus 15 dbi, and 15 dbi versus 26 dbi delayed timing groups, the animals received the first AAV injection in one side of BLA on day 0, then the second AAV injection in contralateral BLA and then the third injections for CAV-2 in both hemispheres of mPFC on different days according to the dbi required.

For optic fiber implantations in BLA, CAR/GCaMP6f-expressing virus AAV9-hSyn-DIO-[hCAR]_{off}[GCaMP6f]_{on}-W3SL and control virus AAV9-hSyn-Flex-GCaMP6f-WPRE-SV40 were injected into opposing BLAs on Day 0. At Day 7-8, CAV-Cre was injected

bilaterally into mPFC. The craniotomies were covered by low viscosity silicone elastomer sealant (Kwik-Cast, World Precision Instruments) temporarily and then adhesive cement (C&B MetaBond, Parkell) was applied on the skull surface except the craniotomies. After the adhesive cured, the Kwik-Cast sealant was removed from the craniotomies to expose the brain surface. The optic fibers (Doric lenses, 400 µm core diameter, NA 0.48) were gently lowered into the brain to the depth of BLA bilaterally or only at CAR+ hemisphere. Once in place, the optic fibers were secured to the skull by multiple layers of Vitrebond Plus light cure glass ionomer liner/base (3M ESPE) and dental acrylic (Lang Dental). Finally, a titanium head-bar was attached to the frontal plate for head-fixation. Then animals received a subcutaneous injection of analgesic solution (Ketoprofen, 5 mg/kg). Three days' postoperative monitoring period were applied during the recovery of animals. Mice were allowed three weeks after fiber implantation for recovery and fully expression of GCaMP6f.

Animal Behavior Training and Fiber Photometry

Mice were trained in a Pavlovian, odor-cued behavioral task to assess how mPFC-projecting BLA neurons respond to reward (water delivery), punishment (air puff) and to novel odor stimuli paired with reinforcement. Mice were water-restricted prior to training to achieve 85%–90% of body weight. To habituate mice to head-fixation, un-cued water reward (5 µL) was delivered at randomized intervals (exponential, mean = 3 s) for 1 or 2 sessions and licking behavior monitored using a custom lickometer. Subsequently, mice were trained in a Pavlovian task in which unique odor stimuli were paired with either reward or punishment. Odor 1 was isoamyl acetate, odor 2 was ethyl tiglate. Odors were diluted in mineral oil and delivered at a final concentration of 1% using a custom olfactometer controlled by an Arduino Uno microprocessor. Each photometry trial consisted of a 4 s baseline period, a 1 s odor stimulus, a 1 s delay, reward (8 µL) or punishment (0.2 s air puff), and a 4 s post-outcome period of photometry recording. Trials were separated by a randomized interval (exponential, mean = 6 s).

Initially, mice were trained in a Pavlovian task wherein the presentation of Odor 1 predicted water reward with 90% probability. Within 1-2 sessions animals developed anticipatory licking for Odor 1 (early sessions). After a few training days, the same animal was trained in a second task in which half of the trials were still Odor 1-Water trials, in the other half of the trials Odor 2 was delivered and signaled aversive air puff with 50% probability (late sessions).

For fiber photometry, a 490nm LED light source (M470F3 Thorlabs) was collimated via an aspheric condenser (ACL25416U Thorlabs), passed through an excitation filter (ET470/24M Chroma), bounced off a dichroic mirror (T495LPXR Chroma), and launched into a 400µm core, 0.48NA fiber patch cable using an aspheric objective lens (A240TM-A Thorlabs). GCaMP6f fluorescence excitation and detection were both accomplished through one multimode optical fiber. Then fluorescence was passed through an emission filter (ET525/50M Chroma), focused with a plano-convex lens ($f = 30$ LA1805-A Thorlabs), and collected using an amplified photodiode (IM 2151 New Focus). The GCaMP6f signal was amplitude-modulated by sinusoidally varying the command voltage of the LED driver (LEDD1B Thorlabs) and decoded *in silico* (Cui et al., 2013; Lerner et al., 2015). Data were acquired using a data acquisition card (PCIe-6321 National Instruments) and analyzed using custom MATLAB code. Olfactometer, photometry data acquisition, and behavioral monitoring were controlled and synchronized using a flexible, open-source master controller interfacing with MATLAB (Bpod State Machine, <https://sites.google.com/site/bpoddocumentation/>).

For correction of the transient (~1 s) fluorescence decay evident at the beginning of each trial, an exponential curve was fit to the mean, baseline period (0-4 s) fluorescence curve and subtracted from each trial. For each trial, fluorescence signals were normalized by calculating the z-score as $(F - \text{mean}(F)) / \text{standard deviation}(F)$, where the mean and standard deviation was taken from a 4 s baseline acquisition period preceding odor cue delivery. .

Immunostaining, TUNEL Staining, and Immunoblotting

Animals were deeply anesthetized with 0.14 g/kg sodium pentobarbital. Intracardial perfusion was performed with saline followed by 4% paraformaldehyde (PFA). The brain was removed from the skull, post-fixed in 4% PFA overnight and precipitated in 30% sucrose solution. Coronal brain slices were sectioned by using a Cryostat (Leica) at 30 µm thickness for mice and 40 µm thickness for rats.

Sections were blocked in PBS containing 5% bovine serum albumin and 0.3% Triton X-100 for 1 hr at room temperature, followed by incubation overnight at 4°C with primary antibodies: Goat anti-HA (Abcam Cat# ab9134, RRID: AB_307035, 1:500); Mouse anti-HA (Abcam Cat# ab18181, RRID: AB_444303, 1:500); Rabbit anti-RFP (Rockland Cat# 600-401-379, RRID: AB_2209751, 1:2000); Rabbit anti-GFP Alexa Fluor 488-conjugated (Molecular Probes Cat# A-21311, RRID: AB_221477, 1:500); Mouse anti-GFP (Santa Cruz Biotechnology Cat# sc-9996, RRID: AB_627695, 1:500); Mouse anti-Myc 9E10 (Santa Cruz Biotechnology Cat# sc-40, RRID: AB_627268, 1:1000); Rabbit anti-Cre (Millipore Cat# 69050-3, RRID: AB_10806983, 1:500); Rabbit anti-mCherry (Abcam Cat# ab167453, RRID: AB_2571870, 1:500); Chicken anti-mCherry (Novus, NBP2-25158, RRID: AB_2636881, 1:500); Chicken anti-TH (Abcam Cat# ab76442, RRID: AB_1524535, 1:500). The next day after washes in PBS, sections were incubated with Alexa Fluor conjugated secondary antibodies (Invitrogen/Molecular Probes, 1:500) at room temperature for 2 hr. After washing, the sections were counterstained with DAPI and mounted (Electron Microscopy Sciences, 17989-61).

Potential apoptosis of neurons at viral injection sites in the striatum was examined using the TUNEL assay kit (Roche, 11684795910) according to the manufacturer's manual. A positive control was added following manufacturer's manual by incubating brain sections with DNase I to induce DNA strand breaks, prior to labeling procedure. Viral injection sites were recognized by the co-injected CTB.

For the investigation of the offset pattern of CAR, primary mouse hippocampal cultures were transfected with AAV-DIO-{mCAR}_{off}{ChR2}_{on} plasmid by electroporation. After 7 days of expression, cells (4E5) were infected by CAV-Cre (8E8 pp) with an infection rate of near 100% (data not shown), and then collected at different post-infection days. Western blots were carried out according to standard protocols. The following antibodies were used: Rabbit anti-Cre (Millipore Cat# 69050-3, RRID: AB_10806983, 1:1000); Mouse anti-Myc 9E10 (Santa Cruz Biotechnology Cat# sc-40, RRID: AB_627268, 1:1000); Mouse anti-HA (Abcam Cat# ab18181, RRID: AB_444303, 1:1000); Rabbit anti-tubulin (Abcam Cat# ab179512, 1:2000). Immunoblot results were quantified using ImageJ.

QUANTIFICATION AND STATISTICAL ANALYSIS

Control and CAR-expressing AAVs were randomly injected into opposing hemispheres during viral injection procedure. This information (control or CAR+, delay duration before injection, and the hemisphere) was coded and hidden from the experimenter afterward for all steps of the immunostaining, imaging, and cell counting. The experimenter was de-blinded after cell counts were done. For all morphological analyses, contralateral sides on the same brain slice were always paired and processed together with same settings. For stereological measurements of the number of immuno-positive cells, one out of every six sections were selected for immunostaining and counting (2-3 sections for BLA, 3 sections for VTA per mouse and 5-6 sections for vCA1 per rat). Z stack images of the regions of interest were collected on a Zeiss 710 LSM confocal microscope with a 10 × Plan-Apochromat objective. For quantification of synaptic puncta, images were acquired with 63 × objective at 2 × zoom. TUNEL staining images were acquired with 20 × objective. Images were analyzed in a blinded fashion by using Image-Pro Plus software (Media Cybernetics, RRID: SCR_007369) for automated cell counting. For each image, the region of interest was outlined from DAPI channel. Images within this region for each channel were threshold-processed to remove the noise pixels arising from general fluorescence background and clusters of continuous pixels above the threshold were identified as cells. The number of cells above a threshold were automatically counted by the software. To validate the automated counting, for some of the samples manual counting was also performed blinded to the experimental conditions. We found that automated and manual counts were similar. All measures of CAV-2 infectivity were normalized to retrograde tracer CTB or Retrobeads. Paired comparisons between opposing hemispheres are provided in each animal.

For all experiments, the statistical differences were computed by using Mann-Whitney U test (for two groups) and one-way ANOVA followed by Tukey's multiple comparison tests (for three or more groups). Statistical analyses were carried out using GraphPad Software. n values represent the number of animals, unless otherwise specified. At least three animals were used for each experimental condition. The statistical parameters are reported in Figures and Figure Legends as mean ± SEM, and statistical significance was set at *p < 0.05, **p < 0.01, ***p < 0.001.

DATA AND SOFTWARE AVAILABILITY

The accession numbers for the sequences of all recombinant AAV constructs developed in this paper are Addgene: 111386-111397.